

Controlling parameters for normal and shear behaviour of rock fractures-a study of direct shear test data from SKB

Hanna Melin



Master of Science Thesis
Stockholm, Sweden 2012



**KTH Architecture and
the Built Environment**



**KTH Architecture and
the Built Environment**

Controlling parameters for normal and shear behaviour of rock fractures – a study of direct shear test data from SKB

Hanna Melin

Master of Science Thesis 12/05
Division of Soil and Rock Mechanics
Department of Civil Architecture and the Built Environment

Stockholm, 2012

Master of Science Thesis 12/05
Division of Soil and Rock Mechanics
ISSN 1652-599X

tear down the mailbox, rip up the floor
smash out the windows and knock down the door
...
we're gonna rock (hey rock) rock this fracture
we're gonna rock this fracture tonight

Bill Haley & His Comets

Abstract

The deep mining and civil engineering industry need to perform rock stability analyses during excavation projects. The stability is mainly controlled by the shear strength of the rock fractures, which are the weakest point of the rock mass. In turn, the shear strength is governed by the mechanical properties of the fractures. It is both time and cost demanding to determine the properties of the rock fractures in laboratory. Also, the interpretation of the results requires a deep understanding of the normal and shear behaviour of rock fractures.

This study aims to investigate if it is possible to determine the peak shear strength of rock fractures by merely estimating fracture parameters during field mapping and core logging.

SKB supplied test results on drilled bore cores from site investigations in Forsmark and Laxemar for deep nuclear waste deposits. SKB generated data of high quality and in large quantity, which made it very valuable for the purpose of the study.

The study begins with a literature review and an interaction matrix, clarifying the relationships between mechanical properties and affecting parameters of rock fractures. The predicted relationships of the parameters are then tested in an analysis based on the compiled data from SKB.

The results show that the peak friction angle, the residual friction angle and the dilation angle are possible to approximate for open granite fractures in deep mining projects.

Further on, the study proposes that the joint matching coefficient is included in the field mapping and core logging since it has a strong influence on the mechanical behaviour of the fracture, notably the normal and shear stiffness. Finally, the study questions estimations of JRC on small samples.

Keywords: open fractures, shear strength, mechanical parameters, basic friction angle, friction angle, dilation angle, stiffness, roughness, joint matching coefficient, deep mining

Summary

Difficulties in determining the stability of rock masses in excavation projects has motivated a study of the peak shear strength of rock fractures. The shear strength is the controlling factor of failure modes such as sliding on the fracture surfaces. The mechanical properties of a fracture govern the shear strength but they are time and cost demanding to determine in-situ. Moreover, the normal and shear behaviour of rock fractures needs to be profoundly understood to enable an accurate interpretation of the results.

The objective of this study is to produce a guide of engineering use in the determination of the peak shear strength of rock fractures. The investigation concerns the possibilities of determine the mechanical behaviour of rock fractures from the field mapping and core logging alone. In order to obtain this, data compilation of shear tests has been performed together with analyses of the data from field mapping and core logging.

SKB has provided quantitative and qualitative test results from drilled bore cores, deriving from the site investigations for deep nuclear waste deposits in Forsmark and Laxemar. In total, data of 41 direct shear tests is combined with data from tilt and UCS tests, core logging and field mapping. The samples used in the tests come from bedrock that consists of mostly granitic material, open fractures and weathering conditions that varied from fresh to moderately altered.

The study presents an interaction matrix that explains the connections between the mechanical properties and the affecting parameters from the field mapping of the rock fracture. An influence analysis is based on the data compilation. It investigates the interactions from the matrix by plotting the data.

The findings of the study are that the peak friction angle, the residual friction angle and the dilation angle are possible to roughly estimate for rock fractures of the same kind of environment (granitic rock and open fractures) for deep mining projects.

Both the literature study and the influence analysis indicate that it is difficult to give guidelines to civil engineering projects where the mechanical properties are subjected to a significant scale effect in low stress conditions.

Also, the study found that the subjective estimation of JRC from field mapping and core logging is questionable. One possible reason for this might be the problems of detecting the intermediate scale of the roughness on drill cores. Finally, the study suggests comprising the joint matching coefficient in the field mapping and core logging at all time.

Preface

This master level degree project was carried out from August 2011 to December 2011 at the Department of Civil and Architectural Engineering, Royal Institute of Technology (KTH).

I am tremendously grateful to my supervisors, Fredrik Johansson, for his genuine support and guidance throughout my research work, and to Diego Mas Ivars, for initiating this project. They generously offered both time and explanations, which deeply improved my knowledge and understanding to the world of rock mechanics.

I want to thank my examiner Stefan Larsson for having, in an inspiring way, introduced me to geotechnical engineering during my education at KTH.

I also wish to express my sincere gratitude to SKB for providing the material, to Malin Johansson, who help me many times with data searching and deliverance, and to Lars Jacobsson at SP, for explaining the procedure of the experiments and the meaning of the results.

Last but not least I am so very thankful to those believing in my capacity through the civil engineering education and especially for supporting me during the last troublesome period. Thanks to my parents, my brother and my sister, and to my friends, for your tireless listening and priceless care.

Stockholm, December 2011

Hanna Melin

Notations

Latin upper case letters

E	Young's modulus of elasticity (Pa)
K_n	normal stiffness (Pa/mm)
K_s	shear stiffness (Pa/mm)
JRC	joint roughness coefficient
JCS	joint wall compressive strength (Pa)

Latin lower case letters

Δu_n	normal displacement (m)
Δu_s^p	plastic shear displacement (m)
c_p	peak cohesion (Pa)
c_{res}	residual cohesion (Pa)
j	Schmidt joint rebound number (wet and weathered joint surface)
J	Schmidt rock rebound number (fresh, sawn and dry joint surface)
i	peak dilation angle ($^\circ$)
s_n	asperity failure component ($^\circ$)

Greek lower case letters

σ_{ci}	unconfined compressive strength (Pa)
σ'_n	effective normal stress (Pa)
τ	peak shear stress (Pa)
τ_{res}	residual shear stress (Pa)
ϕ	peak friction angle ($^\circ$)
ϕ_b	basic friction angle ($^\circ$)
ϕ_{res}	residual friction angle ($^\circ$)

Contents

Abstract	i
Summary	iii
Preface	v
Notations	vii
1 Introduction	1
1.1 Background	1
1.2 Aim	2
1.3 Methodology	2
1.4 Limitations of the thesis	2
2 Literature review	3
2.1 Rock mechanics.....	3
2.2 Mechanical properties of rock fractures	3
2.2.1 Peak friction angle	4
2.2.2 Residual friction angle	5
2.2.3 Basic friction angle	6
2.2.4 Dilation angle.....	7
2.2.5 Normal stiffness.....	8
2.2.6 Shear stiffness	9
2.3 Parameters affecting the mechanical properties of rock fractures.....	10
2.3.1 Unconfined compressive strength of intact rock	10
2.3.2 Effective normal stress	10
2.3.3 Roughness	10
2.3.4 Aperture	11
2.3.5 Scale.....	12
2.4 Additional parameters	14
2.4.1 Young's modulus	14

2.4.2	Weathering degree	14
3	Methodology	15
3.1	Introduction	15
3.2	Interaction model and analysis	15
3.2.1	Influence of compressive strength and effective normal stress	16
3.2.2	Influence of roughness	17
3.2.3	Influence of aperture	17
3.2.4	Influence of scale	17
3.3	Data compilation	18
3.3.1	Derivation of the parameters	18
3.3.2	Quality check of data	19
3.3.3	Limitations of data	19
3.4	Presentation of data	20
4	Results	21
4.1	Data compilation	21
4.2	Influence analysis	22
4.2.1	Peak and residual friction angle	22
4.2.2	Asperity failure component	26
4.2.3	Basic friction angle	27
4.2.4	Dilation angle	28
4.2.5	Normal and shear stiffness	31
5	Discussion	36
6	Conclusions	39
6.1	General conclusions	39
6.2	Suggestions for future research	40
	Bibliography	41
	Appendix A	43

1 Introduction

1.1 Background

Stability analyses of rock excavation projects must satisfy high claims of both safety and profitability. Depending on the depth of the project, the normal stress level differs considerably and therefore also the behaviour of the rock mass. It is thus necessary to distinguish between projects of low stresses in civil engineering (tunnelling and open pit projects) and the higher ones in the deep mining industry.

The rock mass consists of intact rock and fractures. Sliding on the fractures is the most frequent stability failure and is caused by failing shear strength between the fracture surfaces. The normal and shear behaviour of a fracture is governed by its mechanical properties: friction angles, dilation and stiffness quantities. In turn, the mechanical properties are affected by other variables, like normal stress, material strength, roughness, scale and aperture of the fracture.

In both civil engineering and mining industries, carrying out laboratory tests on intact rock samples (UCS, triaxial, Brazilian tests) is regular practice. However, direct shear tests on rock fractures are commonly overlooked and decisions about fracture behaviour have to be taken based solely on fracture mapping data, core logging data and site observations. In these situations, reliance has to be put on empirical models based on site data.

At present, there is still no definitive agreement on how the mechanical properties and the affecting parameters are interacting with each other. It is therefore valuable to produce a systematic study with high-quality laboratory data. The study aims to distinguish how the mechanical behaviour is associated with key variables found during field mapping and core logging. In the opinion of the author, any additional data that helps the understanding of fracture behaviour to move forward is of great value to the rock mechanics community.

This research study was initiated by ITASCA Consultants AB, in collaboration with the Division of Soil and Rock Mechanics at KTH. It undertakes to produce a straightforward and accessible analysis of the parameters controlling the normal and shear behaviour of rock fractures. By deepening the understanding of fracture behaviour, the study benefits equally civil engineering and deep mining projects by the possibility of reducing time and cost losses as well as preventing future accidents.

The thesis consists of three parts that begins with a literature review on important research works of rock fracture properties. Next, the method includes an interaction model, a data compilation and an analysis of the influences between the fracture properties and affecting parameters. The last part presents results and discussion.

1.2 Aim

The objective of this thesis is to examine the possibilities of predicting the peak shear strength of rock fractures based on the affecting parameters at the specific project site. The investigation is based on a compilation of existing direct shear tests data together with results from field mapping and core logging.

1.3 Methodology

To achieve the aim of the thesis, the methodology comprises three stages:

- Compiling quantitative and high-qualitative data from direct shear test results, provided by Swedish Nuclear Fuel and Waste Management Co, SKB.
- Generating an interaction model from important research work within the field of rock mechanics, which explains the relations between the mechanical properties and the affecting parameters of rock fractures.
- Producing an influence analysis of the normal and shear behaviour of rock fractures by presenting the shear test data against data from field mapping and core logging of affecting parameters in several different plot templates.

1.4 Limitations of the thesis

The scope of the thesis lies within unfilled and open rock fractures in granitic rock. The data derives solely from direct shear tests and core logging/field mapping from SKB's publications and data base SICADA.

The conclusions of the thesis concern therefore exclusively environment and conditions similar to the data from SKB's bore cores in Forsmark and Laxemar.

2 Literature review

2.1 Rock mechanics

In rock mechanics, the rock mass is defined as an aggregate of blocks separated by fractures (Goodman et al., 1968). As failure occurs at the weakest point of the rock mass, the properties of the rock fracture are of greatest interest when investigating shear failure analysis (Alejano and Alonso, 2005).

Fractures form when stresses are exceeding the durability of a rock material. The primal properties of the fracture depend on the direction and quantity of the stresses as well as the constitution of the rock material (Zhao, 1997). These properties vary in terms of long/short, wide/tight, inclined/planar and singular/multiple. A rock fracture is defined as two rough surfaces, separated by an opening between them.

The strength of the fracture walls depends mostly on the actual rock type but as the time goes, erosion and movements affect the fracture wall surfaces and the aperture. The shape of the asperities on the fracture surface, the roughness alteration, the degree of dilation, the matedness of the fracture walls and, if present, the features of a filling material are all constantly changing parameters (Hoek, 2007).

The overall key factor to the normal and shear behaviour of a fracture is the contact area between the fracture walls (Hopkins, 2000). The contact area varies with roughness, aperture and normal effective stress. Also, the rock fracture exhibits an elastic behaviour, governed by the normal and shear stiffness. At low normal stress, shearing along the fracture let the asperities on the joint surfaces ride up onto each other. At higher stresses, failures involve shearing through the asperities (Goodman et al., 1968).

In order to describe the normal and shear behaviour of a rock fractures, two groups of variables are identified: mechanical properties and affecting parameters. The mechanical properties are friction angles, dilation angle, apparent cohesion together with normal and shear stiffness, which are all determined through laboratory tests. The affecting parameters, such as alteration, aperture and roughness, are estimated during field visits. They modify the mechanical properties and thus the normal and shear behaviour of the fractures.

2.2 Mechanical properties of rock fractures

In this literature review, the definition and the importance of the following mechanical properties are investigated: the peak and residual friction angles, the basic friction angle, the dilation angle and the normal and shear stiffness.

2.2.1 Peak friction angle

The peak friction angle is a measure of the maximal shear resistance of a fracture. The shear force required to initially displace a fracture equals the effective normal stress multiplied by the tangent of the peak friction angle plus the cohesion, see equation 2.1. A larger peak friction angle thus gives a greater shear resistance.

$$\tau = c_p + \sigma'_n \cdot \tan(\phi) \quad (2.1)$$

Where,

- τ is the peak shear strength.
- σ'_n is the effective normal stress acting on the fracture.
- ϕ is the peak friction angle.
- c_p is the peak cohesion.

The peak friction angle is typically established through a direct shear test. The test is performed on bore core samples, which reflect the site-specific resistance to shear displacement of the natural fractures. During the direct shear test, the fracture is positioned horizontally and exposed to a constant normal stress (Goodman, 1989).

In civil engineering, the cohesion is usually considered to be zero as a conservative measure in order to not overestimate the shear strength of a rock fracture in low stresses. Instead, the friction angle is defined as the secant between the shear and normal stress. However, an apparent cohesion can be accounted for by approximating the peak values of the direct shear tests into a linear fit, i.e. the Mohr-Coulomb approach, see Figure 2.1.

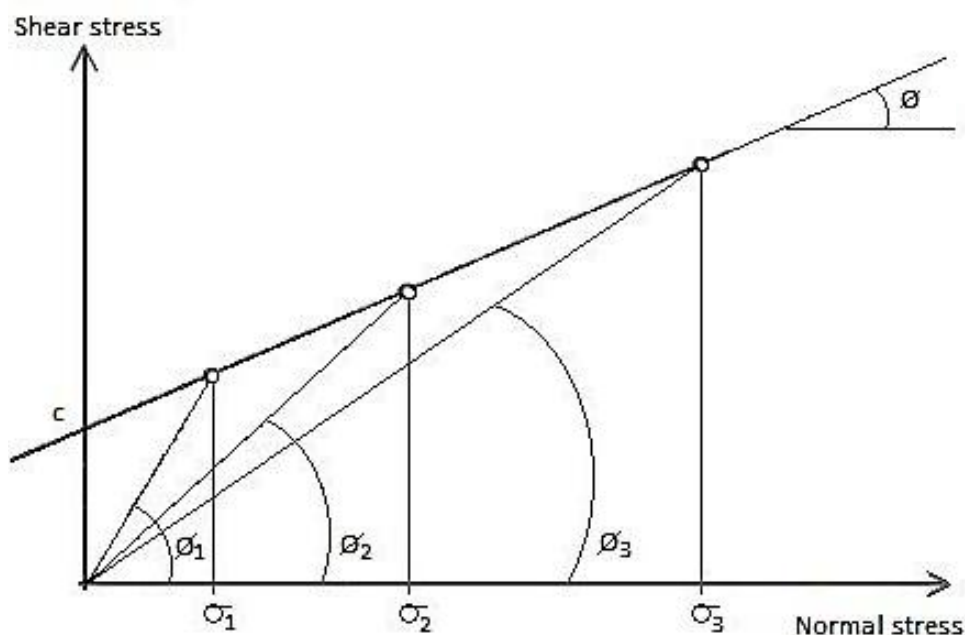


Figure 2.1: Illustration of the two methods to define the shear strength. The straight lines from the origin are defined as secants between the shear and normal stress. The angle of each line presents the friction angle that belongs to a certain applied normal stress. The linear fit of several tests represents the Mohr-Coulomb approach with an apparent cohesion and friction angle.

Barton (1973) suggested a criterion to estimate the peak shear strength by introducing the roughness component, JRC, and the joint wall strength, JCS, as functions of the normal stress. The envelop of the failure criterion obtains an appearance of a slightly curved line, representing the gradually changing shear strength due to decreasing JRC and JCS over high stresses.

Furthermore, Barton and Choubey (1977) replaced the formerly used basic friction angle with the residual friction angle on the grounds that it covers the influence of saturated and weathered fracture surfaces, see equation 2.2.

$$\tau = \sigma'_n \cdot \tan(\text{JRC} \cdot \log_{10} \left(\frac{\text{JCS}}{\sigma'_n} \right) + \phi_{res}) \quad (2.2)$$

Where,

JRC is the fracture roughness coefficient.
 JCS is the fracture wall compressive strength.
 ϕ_{res} is the residual friction angle.

In Figure 2.1, it is possible to choose the stress level that corresponds to the actual normal stress at the project site. This method is appropriate both for civil engineering and deep mining industry. The Mohr-Coulomb method obtains a linear fit of the peak shear strength over several stress states and provides a mean value on the shear strength.

The peak friction angle is generally considered to be composed by three parts; the dilation component (chapter 2.2.4), an asperity failure component and the basic friction angle, see equation 2.3 (Bandis et al., 1983). The two first parameters account for the shear resistance due to roughness of the fracture surfaces and the shearing or crushing of the fracture wall asperities. The basic friction angle describes the contribution from a macroscopic smooth but microscopic rough surface, see chapter 2.2.3 (Johansson, 2009).

$$\phi = i + s_n + \phi_b \quad (2.3)$$

Where,

i is the dilation angle.
 s_n is the asperity failure component.
 ϕ_b is the basic friction angle.

When the peak friction angle of a saturated and weathered rock fracture is considered, the basic friction angle should be replaced by the residual friction angle, see chapter 2.2.2 (Barton and Choubey, 1977).

2.2.2 Residual friction angle

It exist two methods in rock mechanics to define the residual friction angle. They are fundamentally different and it is important to separate between them.

During the direct shear test, the required shear force to cause displacement decreases to a residual value after the peak. The residual shear force remains more or less constant even during large displacements, see Figure 2.2. This friction angle is defined as the residual friction angle (Hoek, 2007).

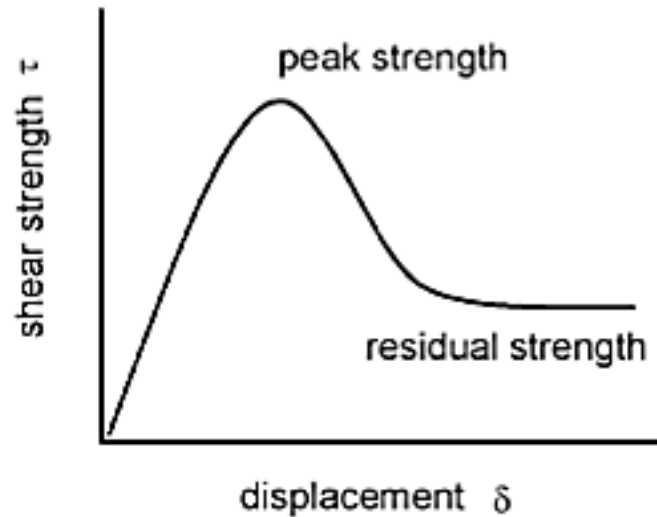


Figure 2.2: The shear strength decreases after the peak and remains constant during further displacement: the residual state (Hoek, 2007).

Another definition has been suggested by Barton and Choubey (1977). They propose to use the residual friction angle instead of the basic friction angle in order to account for saturated and weathered fracture surfaces. This residual friction angle is estimated, based on empirical investigations, using equation 2.4 suggested by Barton and Choubey (1977):

$$\phi_{res} = (\phi_b - 20^\circ) + 20 \cdot (j/J) \quad (2.4)$$

Where,

- j is the Schmidt rebound number on a wet and weathered surface.
- J is the Schmidt rebound number on a dry, sawn and fresh surface.

J and j are quantities of the hardness of the rock material on dry, sawn and unweathered respectively wet and weathered fracture surfaces. They can be estimated in field by the method of the Schmidt hammer (Barton, 1973). In fresh conditions, J and j are similar which gives a j/J ratio of one and thereby, the equation 2.4 shows that the angles are equal. This study uses the former definition where the residual friction angle is derived from direct shear test.

2.2.3 Basic friction angle

The basic friction angle is the friction angle that originates from macroscopic smooth but microscopic rough surface. The value of it is correlated to specific rock types. In general, the basic friction angle is determined by tilt testing. Thus, the basic friction angle can be interpreted as a measure of the prime shear resistance of a material.

A type of tilt test called a core-to-core test can be used to establish the basic friction angle of a rock material. The test is performed with three dry and sawn-smooth rock cores, where two cores are placed in the bottom and the last one lies on top. During the test, the

inclination of the samples increases until the one on top begins to slide under its own weight (Chryssanthakis, 2003).

2.2.4 Dilation angle

The shearing of a rock fracture may be accompanied by dilation, i.e. a volume increase when the fracture is forced to open up due to sliding over the asperities on the rock walls during the horizontal displacement.

The controlling factors of the dilation are the strength of the rock material, the angle of the asperities and the normal load (Goodman et al., 1968). If the walls have an absolutely smooth surface, no dilation occurs.

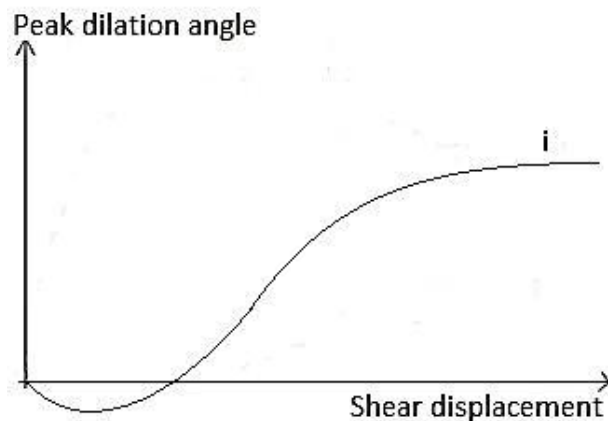


Figure 2.3: The dilation angle decreases at first due to compression of the fracture (Seidel and Haberfield, 1995). After that, dilation occurs due to sliding over the asperities.

Dilation is only assumed to start once the shear behaviour of the fracture turns plastic, i.e. when shearing over the asperities begins. The dilation angle decreases at first due to compression of the fracture, see Figure 2.3.

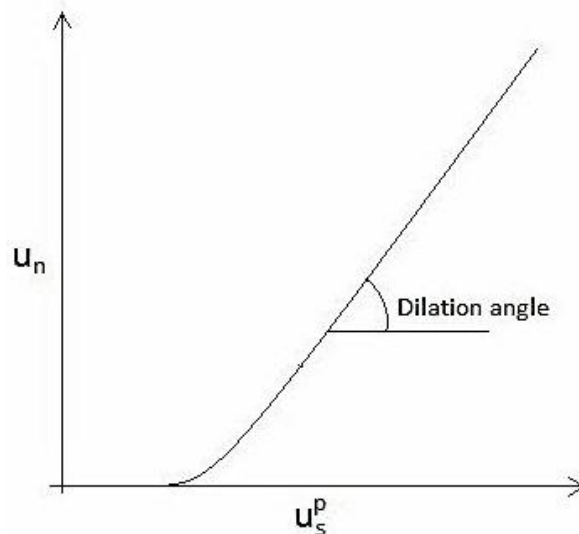


Figure 2.4: The plot of the normal and plastic shear displacement of a fracture exposed to a direct shear test. The dilation angle is the slope of the curve. Positive normal displacement means an increase in aperture.

During a direct shear test, the normal and shear displacements are recorded and plotted, see Figure 2.4. The slope of the plot represents the dilation angle, see equation 2.5.

$$\Delta u_n = \Delta u_s^p \cdot \tan(i) \quad (2.5)$$

Where,

Δu_n is the normal displacement.

Δu_s^p is the plastic shear displacement.

To achieve a horizontal displacement in a rough fracture, a shearing force is required in order to override the asperities. High normal load and large shear displacements cause the dilation angle to decrease when the asperities get sheared off caused by failing durability of the material (Alejano and Alonso, 2005).

$$s_n + i = JRC \cdot \log_{10}(JCS/\sigma'_n) \quad (2.6)$$

The approach of describing the shear strength as a gradually changing event was developed by Barton and Choubey (1977). They suggested that the friction angle that originates from the roughness also is a function of wall strength and normal stresses. Equation 2.6 accounts for the entire roughness contribution, i.e. both the asperity failure component and the dilation angle.

2.2.5 Normal stiffness

The normal stiffness is defined as the ratio of the normal stress and the normal displacement, see equation 2.7. It has the dimension Pascal per millimetre (Zangerl et al., 2008). It is graphically defined as the slope of the stress-displacement curve (Figure 2.5).

$$K_n = \sigma'_n / \Delta u_n \quad (2.7)$$

Where,

K_n is the normal stiffness.

The normal stiffness is strongly connected to the contact area of the fracture surfaces. If the surfaces have no contact, the stiffness is zero, and if the fracture is perfectly mated, the stiffness would be infinite (Hopkins, 2000).

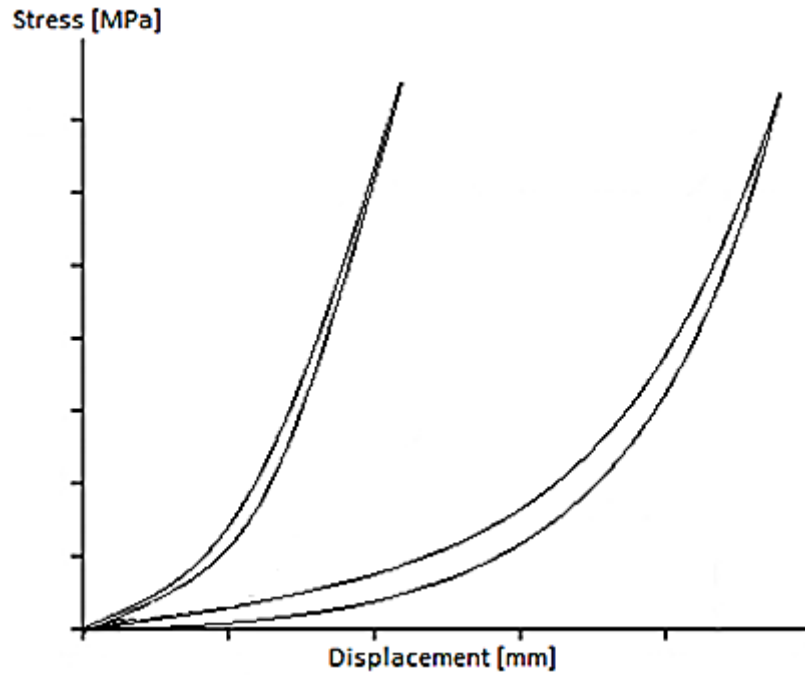


Figure 2.5: During a normal load test, the rock fracture is exposed to several load cycles. The natural condition of the rock fracture is considered to be approached after the first loads and produces a steeper curve (Jacobsson, 2005).

Zangerl et al. (2008) proposed a constant stiffness characteristic that produces a linear approximation, see equation 2.8. This makes it possible to estimate the normal stiffness of a specific fracture at any normal stress by multiplying a selected normal stress by its stiffness characteristic.

$$K_n = (dK_n/d\sigma'_n) \cdot \sigma'_n \quad (2.8)$$

Where,

$dK_n/d\sigma'_n$ is the index of how the stiffness changes in relation to the effective normal stress.

2.2.6 Shear stiffness

The shear stiffness is defined as the slope of the curve from the origin to the measured peak strength. The peak shear stress is divided by the shear displacement in order to obtain the shear stiffness, see equation 2.9.

$$K_s = \tau / \Delta u_s \quad (2.9)$$

Where,

K_s is the shear stiffness.

Therefore, all parameters that affect the peak shear strength will consequently affect the shear stiffness.

2.3 Parameters affecting the mechanical properties of rock fractures

Several affecting parameters have a large impact on the mechanical properties. Also, they affect each other during changing conditions. This chapter offers an explanation and interpretation to each of them in relation to their influence on the shear strength behaviour of a rock fracture.

2.3.1 Unconfined compressive strength of intact rock

The unconfined compressive strength (UCS) of an intact rock material depends on the constitution of present minerals. It is defined as the ability to resist a uniaxial compressive load. To evaluate the strength, a sample undergoes a destructive test where the durability of compression is exceeded and causes fractures in the sample.

The ratio between the normal stress and the uniaxial compressive strength can be assumed to reflect the contact area of the fracture. An increased UCS implies harder asperity material and consequently, a smaller contact area. For natural fractures in granitic rock, the contact area is quite low, even during relatively high normal stresses (Hopkins, 2000).

The strength of the fracture surface material differs depending on the strength of the intact rock and the degree of weathering (Johansson, 2003). If the fracture wall is unaffected by weathering, its strength equals the one of the intact rock. However, if the fracture has suffered from weathering and saturation the strength is decreased. The joint wall compressive strength is usually expressed with the parameter JCS as suggested by Barton (1973).

2.3.2 Effective normal stress

The normal stress that acts on a specific fracture varies with the fracture inclination as well as the depth and the surroundings, for example the weight of the overburden and hydrological conditions (Hoek, 2007). The actual stress that acts on a rock fracture, the effective normal stress, is the difference between the normal stress and the pore water pressure.

When the effective stress that acts on the fracture is decreased, the contact area is reduced, see chapter 2.3.1.

2.3.3 Roughness

The roughness describes the appearance of the joint wall surface. During the formation of the fracture, the walls were shaped according to an interaction between the direction of the stresses and the constitution and structure of the rock crystals. As a result, fracture surfaces are build-up by an undulating landscape of asperities of different angles and sizes. Steep and numerous asperities increase the shear strength (joint wall contact provided). High roughness degree is thus a component that strengthens the shear resistance.

The shearing of a rock fracture happens through two kinds of events. The sliding over asperities results in dilation. The shearing through asperities results in a contribution from the asperity failure component.

The weathering process together with movements of the fracture, affects the roughness degree; it decreases with repeated abrasion and increases with certain chemical erosion. In a small scale, the appearance of the asperities is significant and referred to as the unevenness of the surface. At larger scales, the asperities melt into a waviness of larger undulation and flatter curves (Brown, 1981). When a fracture experiences a low fracture wall compressive strength or high effective normal stress, the asperities will be damaged during shear displacements.

During field mapping, the roughness could be estimated with help from roughness profiles developed by Barton and Chobey (1977). The roughness component used in calculations is called JRC. It can also be back calculated from tilt tests, see equation 2.10.

$$JRC = (\tan(\frac{\tau_p}{\sigma_n}) - \phi_b) / \log_{10} \left(\frac{JCS}{\sigma_n} \right) \quad (2.10)$$

Where,

τ_p is the peak shear strength for a specific effective normal stress.

2.3.4 Aperture

The aperture measures the opening between two fracture surfaces. It depends on the weathering, the relative displacement, effective normal stress, the joint wall compressive strength and the roughness of the fracture.

The matedness and aperture of a rock fractures are inevitably related. If two fracture surfaces fit perfectly, the fracture is matched. On the other hand, as the degree of mismatching increases the aperture of the fracture expands. Zhao (1997) introduced an index to measure the degree of “pattern agreeeness” of the fracture surfaces: the joint matching coefficient (JMC). The index takes both the waviness (large scale) and the degree of roughness (small scale) of the fracture into account (Figure 2.6).

Joint surface roughness (JRC)	Joint waviness matching				
	1	2	3	4	5†
Slickensided (1–3)	1–2	1–3	2–4	2–5	2–5
Smooth (4–7)	2–3	3–4	4–6	5–7	6–9
Rough (8–11)	3–5	4–6	6–8	7–10	19–13
Very rough (12–15)	5–7	6–9	8–11	10–13	13–17
Stepped rough (16–20)	7–10	9–12	11–14	13–17	16–20

†1—very good, 2—good, 3—fair, 4—poor, 5—very poor.

Figure 2.6: The fracture matching coefficient, JMC, is determined from the joint waviness matching and the degree of roughness of the fracture (Zhao, 1997).

Unfortunately, matedness is rarely registered during field mapping, which complicates future studies of its importance.

2.3.5 Scale

The scale parameter is a complex factor to interpret. Tests are usually performed on small scale samples; the result is then approximated on full-scale fracture sizes. However, it has been shown that the normal and shear stiffness as well as the shear strength of the same fracture differs depending on the scale. Laboratory tests have the advantage of being easier and more cost efficient to perform than in-situ tests on larger scales, this is why a method for scale adapting is of large interest.

Small laboratory samples mobilize higher peak shear strength than large samples of the same fracture. The displacement required to mobilize peak strength also increases with larger scale, which indicates reduced shear stiffness (Barton, 1981).

It has been showed that the measured shear strength has the largest reduction from very small scales to intermediate scales (0-3000 cm²). The decrease in shear strength on a larger scale basis is not as affected (Figure 2.7). This means that small scale laboratory tests are not reflecting the actual shear resistance of a fully sized fracture (Yoshinaka et al., 1993).

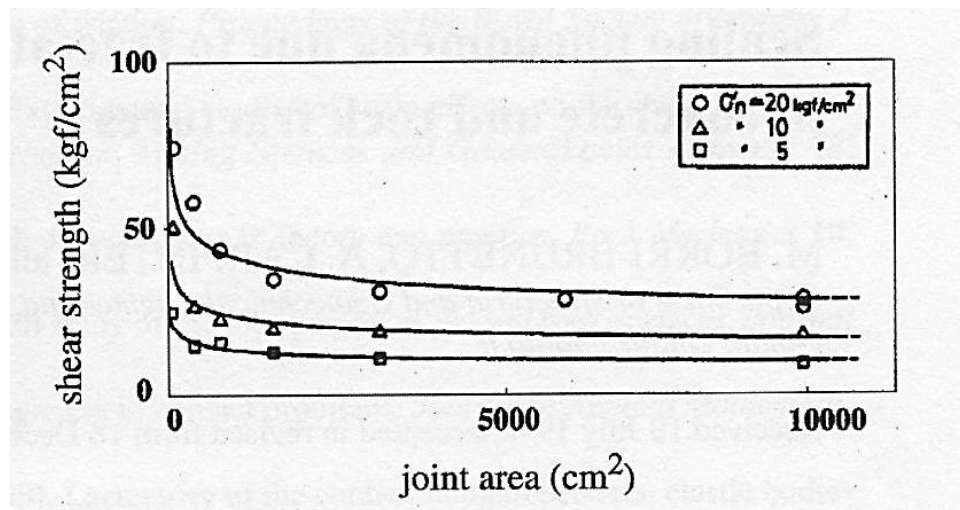


Figure 2.7: Increased sample size results in decreased shear strength, from experimental measurements (Yoshinaka et al., 1993).

Barton and Bandis (1982) suggested a way of scale adjusting the JRC and JCS parameters, see equations 2.11 and 2.12. The subscripts “n” and “o” indicate in-situ block size and laboratory scale of 100 mm respectively.

$$JRC_n \approx JRC_o \cdot \left[\frac{L_n}{L_o}\right]^{-0.02 \cdot JRC_o} \quad (2.11)$$

$$JCS_n \approx JCS_o \cdot \left[\frac{L_n}{L_o}\right]^{-0.02 \cdot JRC_o} \quad (2.12)$$

Where,

L is the average block size in the rock mass, which is assumed to equal the length of the sample.

Fardin (2003) investigated the scale effect on normal and shear stiffness. Exposed to several stress levels, concrete fracture replicas of different sample sizes were examined. The results agree well with the above mentioned findings. The normal and shear stiffness both exhibit decreasing values with larger sample sizes (Figure 2.8).

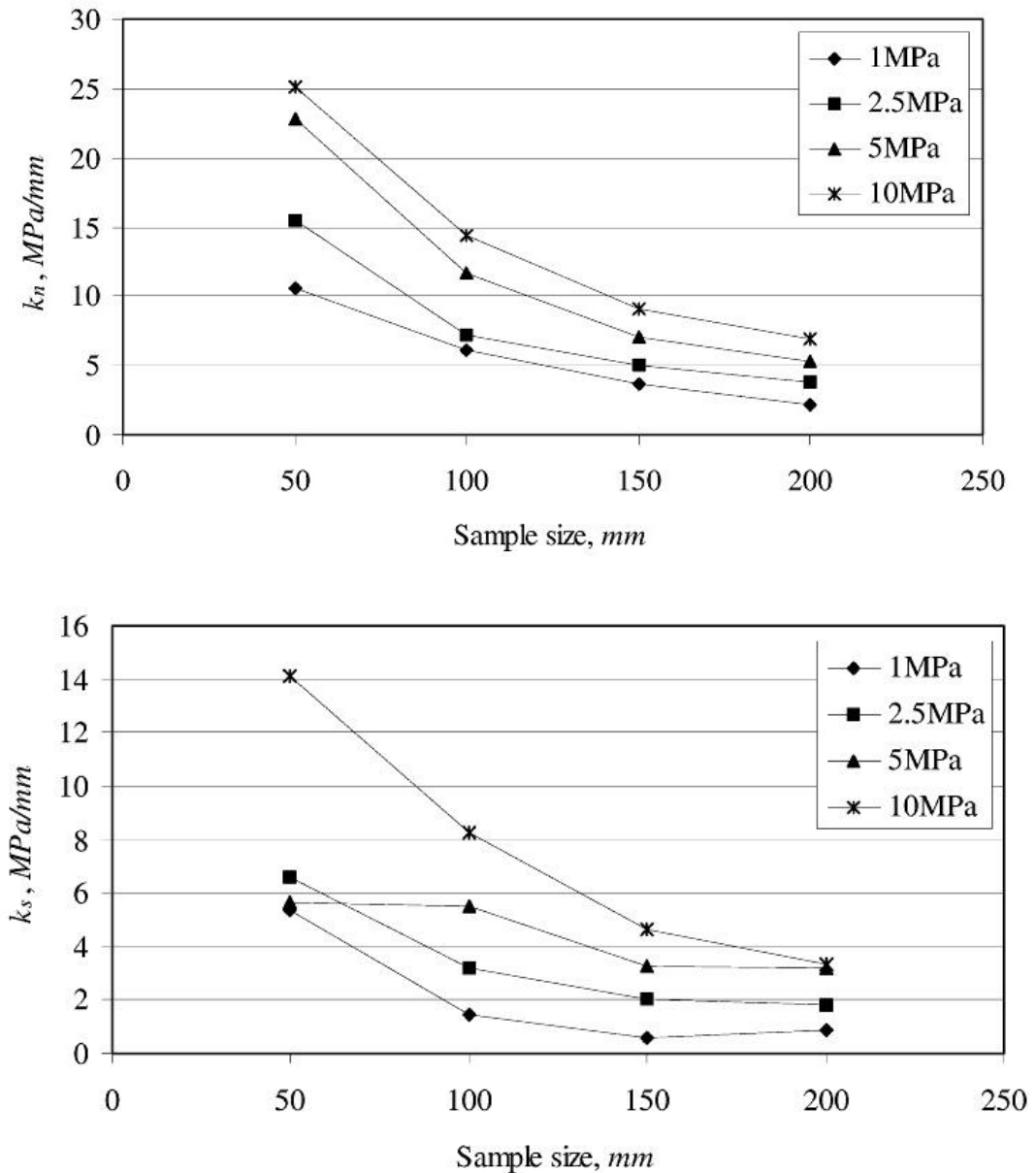


Figure 2.8: A scale effect on the normal and shear stiffness of different sample sizes regardless altering stresses (Fardin, 2003).

Progress has been made to find a transformation model from small scale measured shear strength to estimated large scale shear strength, but it is not yet firmly established (Borri-Brunetto et al., 1998). Barton and Choubey (1977) suggested that the peak shear stiffness could be adjusted to the scale by introducing a factor $100/L$, see equation 2.13.

$$K_s = 100/L \cdot \sigma'_n \cdot \tan(\text{JRC} \cdot \log_{10} \left(\frac{\text{JCS}}{\sigma'_n} \right) + \phi_{res}) \quad (2.13)$$

As the roughness has an important position, an understanding of the roughness at different scales is essential. Seidel and Haberfield (1995) claim that so far the studies of roughness concern only the symptoms and not the cause. They suggest that the problem can be solved with help of the fractal geometry perspective.

2.4 Additional parameters

The Young's modulus and degree of weathering can also have influence on the affecting parameters for both the normal and shear behaviour of fractures.

2.4.1 Young's modulus

Applied normal stress affects the closure of the fracture, which increases the contact area between the walls. The rock material is proposed to act elastically before reaching permanent deformations. As a consequence, in the elastic state, the behaviour is predicted by its Young's modulus property.

Variations of the Young's modulus have an influence on both fracture deformations and normal stiffness. Marache et al., (2008) showed that deformations of fractures as well as changes in the normal stiffness are depending on the Young's modulus of the bulk material.

Hopkins (2000) confirms the importance of the Young's modulus. During normal stress, the asperities are pressed against the opposing fracture wall, deforming not only themselves but the rock material surrounding the asperity. The geometry and configuration of asperities together with the Young's modulus of the material describes more complex deformation behaviour and thus a different stress distribution over the fracture surface. This will affect the actual behaviour of the rock fracture exposed to a shear force.

2.4.2 Weathering degree

The degree of weathering is indirectly accounted for with the JCS, the JRC and the aperture of the fracture. These parameters are disturbed by the weathering process, which progressively modifies the fracture wall landscape, enlarges the aperture or fills the opening with fine particles (Woo et al., 2010).

If the weathering degree is recorded during field mapping, the JCS can be established according to Bandis et al. (1983). The fracture can be classified into fresh, slightly and moderately weathered and weathered. The compressive strength is then reduced to a JCS value depending on the weathering status. The procedure is explained in the chapter of the derivation of parameters (3.3.1).

3 Methodology

3.1 Introduction

Establishing an interaction matrix of the relationship between the mechanical properties and affecting parameters is central in order to analyse relevant data. It acts as a base for an appropriate analytical approach.

Based on data from several studies and projects, SKB was selected to be the only data provider because of the quantity and quality of this data. In this data, almost all mechanical and affecting parameters are available in a satisfactory manner.

The data results come from both laboratory tests and field mapping on drilled bore cores in the region of Forsmark and Laxemar. The bedrock constitutes mainly of granitic rock of medium grain size (1-5 mm). In the laboratory, shear tests, tilt tests and uniaxial compressive strength tests on intact rock were performed.

The methodology consists of the data compilation, the interaction model and the influence analysis. The quality and quantity of the data compilation are of utmost importance in order to produce a meaningful analysis. Based on the expected behaviour in the interaction model between different mechanical and affecting parameters, plots are produced in order to study if trends and expected behaviours could be detected.

In the analysis, focus has been on unfilled and rough fractures.

3.2 Interaction model and analysis

The interaction model investigates how increasing affecting parameters influence the mechanical properties. One should keep in mind that the effects are analysed as isolated events, in reality several things occur at once which makes an analysis much more complicated. The interaction matrix is presented in Table 3.1.

Table 3.1: The interaction model of rock fractures describes how the mechanical properties react to increasing affecting parameters.

INCREASING AFFECTING PARAMETERS					
MECHANICAL PROPERTIES	Unconfined compressive strength, σ_{ci}	Effective normal stress, σ'_n	Roughness	Aperture	Scale
Basic friction angle, Φ_b	Increased Φ_b	unchanged	unchanged	unchanged	unchanged
Peak friction angle, Φ	increased Φ	decreased Φ	increased Φ	decreased Φ	decreased Φ
Dilation angle, i	increased i	decreased i	increased i	decreased i	decreased i
Asperity failure component, s_n	increased s_n	decreased s_n	increased s_n	decreased s_n	decreased s_n
Normal stiffness, K_n	increased K_n	increased K_n	decreased K_n	decreased K_n	decreased K_n
Shear stiffness, K_s	increased K_s	increased K_s	increased K_s	decreased K_s	decreased K_s

In the analysis below, the effects on the mechanical properties from the changes in the affecting parameters are explained and analysed.

3.2.1 Influence of compressive strength and effective normal stress

The basic friction angle depends on the intact rock material. It has been observed that high UCS results in high basic friction angles (Barton, 1973).

The ratio between the effective normal stress and the uniaxial compressive strength reflects the contact area. Increased normal effective stress compresses the fracture, i.e. the aperture reduces and the contact area increases (Hopkins, 2000). A larger contact area means that the peak friction angle decreases. As the fracture gradually closes under the normal load, the closure requires more and more effort in order to compress or crush it further; the normal stiffness progressively intensifies.

The asperities on the fracture surface constitute the main resistance to shear movement, which makes the strength of them significantly important. Consequently, the normal and shear stiffness both grow with a material with higher uniaxial compressive strength (Brown, 1981).

The shear behaviour of the fracture can either be sliding up on the asperities or crushing/shearing through them. Sliding up on the asperities results in an increased dilation angle. In case of extremely high normal stress or weak rock material, the asperities are sheared off with decreased dilation as a result, but with an increased asperity failure component, s_n (Ladaoui and Archambault, 1970).

3.2.2 Influence of roughness

Increased roughness results in more unevenness and waviness along the fracture surfaces. This means that it is harder to generate a shear movement since the fracture walls are forced to open up wider. The dilation angle is hence increased, as well as the peak friction angle. Moreover, the fracture is more difficult to shear because the fracture walls interlock more, i.e. higher asperity failure component and also high shear stiffness. However, the normal stiffness decreases since rougher surface is more likely to be mismatched and therefore, holds more open space to compress (Seidel and Haberfield, 1995).

3.2.3 Influence of aperture

Enlarged aperture decreases the number of contact points, if it is assumed that the contact stress is close to the uniaxial compressive strength. As a consequence, the size of individual contact points between the joint walls increase. An increased size of the contact points results in a lower contribution from roughness (Hopkins, 2000, Wines and Lilly, 2003).

The mechanical parameters of the fractures such as peak friction angle, dilation angle together with normal- and shear stiffness will decrease (Zhao, 1997).

3.2.4 Influence of scale

As previously discussed in chapter 2, it has been shown that larger scale decreases the shear strength of a rock fracture (Fardin, 2003). In a similar manner, mechanical properties excluding the basic friction angle decrease with increasing scale. Low shear strength implies a reduced peak friction angle, and consequently, a reduced dilation angle and asperity failure component. Correspondingly, the shear stiffness decreases as the resistance to shear force is diminished. Most likely, there is also a reduction in the normal stiffness, mainly because there will be larger contact points in larger samples, at least for unmated fractures.

3.3 Data compilation

The data originates from shear, tilt and UCS testing as well as field mapping of drilled bore core samples in the region of Laxemar and Forsmark, Sweden. SKB has provided extracts of desired parameters from the SICADA database and offered explaining reports on the open web data base.

Seven drill holes contained complete data sets of the shear testing, tilt testing, uniaxial compressive strength testing and the field mapping. They are KFM01A, KFM02A, KFM03A, KFM04A, KFM05A in Forsmark and KLX01 and KLX02 in Laxemar (Jacobsson, 2004, Jacobsson, 2005 and Chryssanthakis, 2003).

The shear test results are the point of departure for this analysis that supply the main part of the parameters: peak and residual friction angle, dilation angle, normal stress, normal and shear stiffness, scale and cohesion. Results of the basic friction angle, Young's modulus and the rock type strengths come from the tilt and uniaxial compressive strength testing reports. The field mapping documents contained roughness degree, apertures and alteration descriptions of the fractures in each drill hole.

The shear tests are performed on fracture samples assigned with *secup* and *seclow* units. In order to correlate the characteristics from the other tests, the *secup* and *seclow* units are used as an orientation mark. This represents the upper and lower sampling distance along the drill hole, which is not similar to depth since the drill holes are not always perpendicular to the surface level.

3.3.1 Derivation of the parameters

During shear testing, each fracture sample was exposed to a load of 0.5 MPa, 5 MPa and 20 MPa, i.e. three shear tests for each sample. The three shear tests results enable a Mohr-Coulomb approximation of the peak and residual friction angle and cohesion.

For each normal load, the peak and residual shear forces were also registered individually and plotted through the origin. Equation 3.1 was used to obtain the secant line from the origin to the respectively load, in agreement with Jacobsson (2005).

$$\tau = \sigma'_n \cdot \tan(\phi) \quad (3.1)$$

Where,

- τ is the shear stress.
- σ'_n is the normal stress acting on the fracture.
- ϕ is the friction angle.

The UCS test reports presented the unconfined compressive strength and Young's modulus according to drill holes and rock type. Several tests were performed on every rock type. The median value for both UCS and Young's modulus was selected for this thesis.

The alteration of the fractures was described as fresh, slightly weathered or moderately weathered in the field mapping. Bandis et al. (1983) proposed the ratio σ_{ci}/JCS to be larger than 1.2 for fresh and slightly weathered fractures and between 1.2 and 2 for moderately weathered fractures. The lowest value of each range was chosen; the fresh fractures got a ratio of 1, the slightly weathered a ratio of 1.2 and the moderately weathered a ratio of 2.










Description	Profile	J_r	JRC 200mm	JRC 1 m
Rough		4	20	11
Smooth		3	14	9
Slickensided		2	11	8
	Stepped	2	11	8
Rough		3	14	9
Smooth		2	11	8
Slickensided		1.5	7	6
	Undulating	1.5	7	6
Rough		1.5	2.5	2.3
Smooth		1.0	1.5	0.9
Slickensided		0.5	0.5	0.4
	Planar	0.5	0.5	0.4

Figure 3.1: Converting table of waviness and unevenness profiles into JRC values (Barton, 1987).

The field mapping generated roughness estimations in intermediate (stepped, undulating or planar) and small scale (rough, smooth and slickensided). The JRC values were estimated from Barton's (1987) profile converter for laboratory scale samples (JRC for 200 mm), see Figure 3.1.

The normal stiffness was established through normal load testing, where the sample undergoes two load cycles of 0-10 MPa. The normal stiffness is determined from the second load cycle as the secant of the curve (Jacobsson, 2005).

3.3.2 Quality check of data

A quality check of the data was performed due to difficulties of coherence between the laboratory and field mapping results. The uncertainty concerned the setup and seclow units, which did not accord perfectly in all cases. To ensure that the results from the laboratory tests and field mapping refer to the same fracture, the quality check excludes data that differs more than 10 centimetres in proximity.

SKB performed 41 direct shear tests. It remained 12 direct shear tests after the quality check.

3.3.3 Limitations of data

All parameters have been determined with laboratory tests on drill cores. Since there are no tests performed in other scales, the scale effect is incomparable and therefore excluded from the analysis.

3.4 Presentation of data

Presentation of data has been based on two different plot templates. The first puts the mechanical properties on the y-axis and the ratio σ'_n/σ_{ci} on the x-axis. The data is then divided into different groups according to the size, range or feature of the affecting parameters. For example, the JRC is plotted in series, differentiated by normal loads.

The second template plots the mechanical parameters directly against the affecting parameters, for instance the peak friction angle to the fracture width. Also, in this layout, the affecting parameters are differentiated similarly to the first template.

Table 3.2 presents a list of all plots. The plots of quality checked (QC) data are found in the result section and the plots of all data are found in appendix A. The quality check does not concern the plots of the Young's modulus, since no data from the field mapping is involved. Consequently, they are merely found in the result section.

The uncertainty of the plots in appendix A is too severe to be disregarded since a confident correlation between different tests could not be established. Nevertheless, the result could still be interesting for future studies, provided that the uncertainty is remembered.

Table 3.2: List of presented plots within the study that can be found either in the result section or in appendix A.

Presented plots	QC-data (result section)	All data (appendix A)
ϕ against JRC (separated by σ_n used during direct shear tests)	x	x
ϕ against fracture width	x	x
ϕ against σ_n/σ_{ci} (separated by Young's modulus)	x	
ϕ against σ_n/σ_{ci} (separated by infilling features)	x	x
ϕ against σ_n/σ_{ci} (separated by JRC)	x	x
Mean ϕ_{res} against σ_n/σ_{ci}	x	
S_n against σ_n/σ_{ci}	x	
i against JRC (separated by σ_n used during direct shear tests)	x	x
i against fracture width	x	x
i against σ_n/σ_{ci} (separated by Young's modulus)	x	
i against σ_n/σ_{ci} (separated by infilling features)	x	x
S_n and i against σ_n	x	
K_n against JRC	x	x
K_s against JRC (separated by σ_n used during direct shear tests)	x	x
K_n against fracture width (separated by infilling features)	x	x
K_s against fracture width (separated by infilling features)	x	x
K_n against Young's modulus	x	
K_s against Young's modulus (separated by σ_n used during direct shear tests)	x	

4 Results

4.1 Data compilation

In total, 123 shear tests were compiled. It represents data from 41 fractures in granitic bedrock tested under three different normal stresses. After the quality check of the data compilation, 36 test data from 12 fractures remained.

The fractures vary from fresh to moderately weathered. The most present coating minerals and infilling materials are laumontite, chlorite, calcite, prehnite and pyrite.

The data compilation has been registered in an excel document and is available on request to the author or supervisors of the degree project.

Six rock types are present within the test data: medium-grained metagranodiorite-granite, tonalite, granite-granodiorite, medium-grained granite, Ävrö granite and quartz monzodiorite. Table 4.1 shows the statistical data of the basic friction angle of each rock type from performed tilt tests (Chryssanthakis, 2003).

Table 4.1: Statistical data of the basic friction angle for the present rock types.

Basic friction angle				
Rock type	N° of samples	Mean	Min	Max
Medium-grained metagranodiorite-granite	39	30.5	24	32.7
Tonalite	9	34	34	34
Granite-granodiorite	9	31.7	31.2	32.8
Medium-grained granite	18	29.9	29	32.8
Ävrö granite	45	33.0	32	33.7
Quartz monzodiorite	3	32.8	32.8	32.8

The maximum and minimum values of the Schmidt rebound number for the quality checked samples are shown in Table 4.2.

The estimated condition of the fracture wall (fresh, slightly or moderately altered) from the field mapping did not correspond to the Schmidt rebound number as expected. For example, the moderately altered rock fractures did not exhibit the lowest Schmidt rebound number.

Table 4.2: The maximum and minimum value of the Schmidt rebound number (wet and dry conditions) of the quality checked data.

Schmidt rebound number	N° of samples	Min	Max
j (wet)	36	27.2	42.9
J (dry)	36	44.6	51.8

4.2 Influence analysis

The aim of the influence analysis is to investigate the effect on the mechanical properties due to variations in the affecting parameters. This has been performed with the help of excel plots as previously described. In this section, the plots of the quality checked data are presented and the equivalent ones of all data can be found in appendix A.

The statistical information of each mechanical property includes all data. The statistical information concerns merely the mechanical properties derived from the direct shear tests and are thus not subjected to the incoherence problem of different analyses.

4.2.1 Peak and residual friction angle

In Figure 4.1, the peak friction angle is plotted against JRC and divided in three groups with respect to the normal stress used in the direct shear tests. The plot shows no effect of an increased JRC on the peak friction angle. Figure 4.2 does not either present obvious trend in the plot of the peak friction angle against the fracture width.

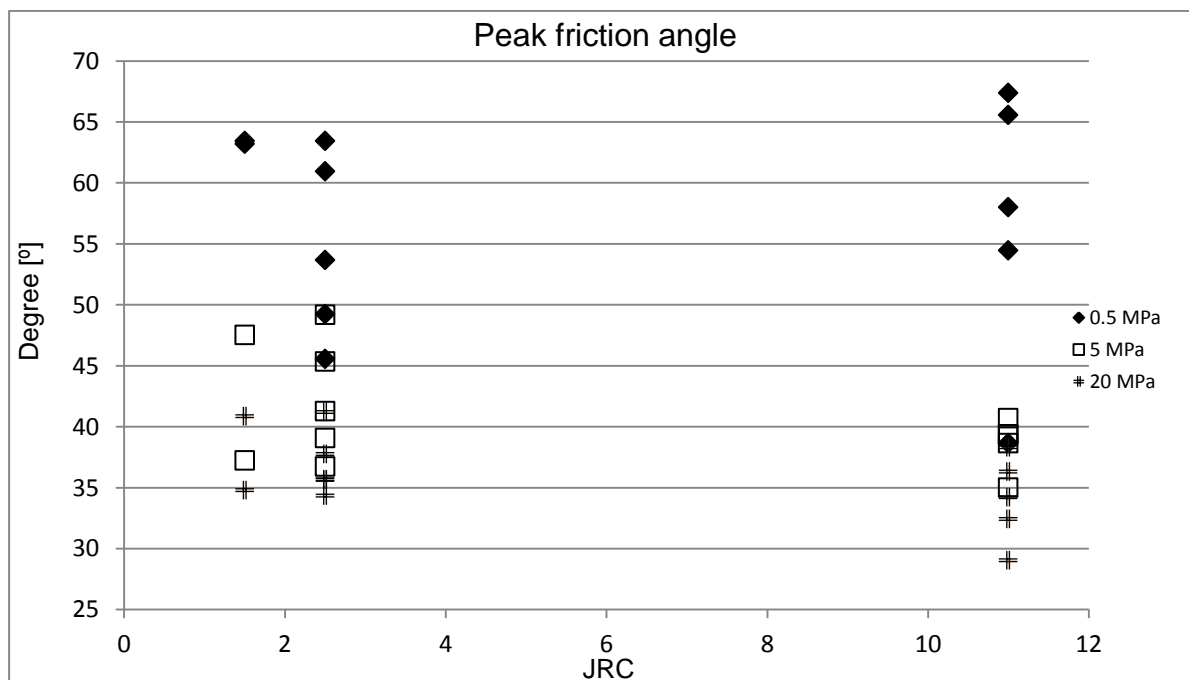


Figure 4.1: The peak friction angle plotted against the JRC, differentiated by the normal stress used during the direct shear tests.

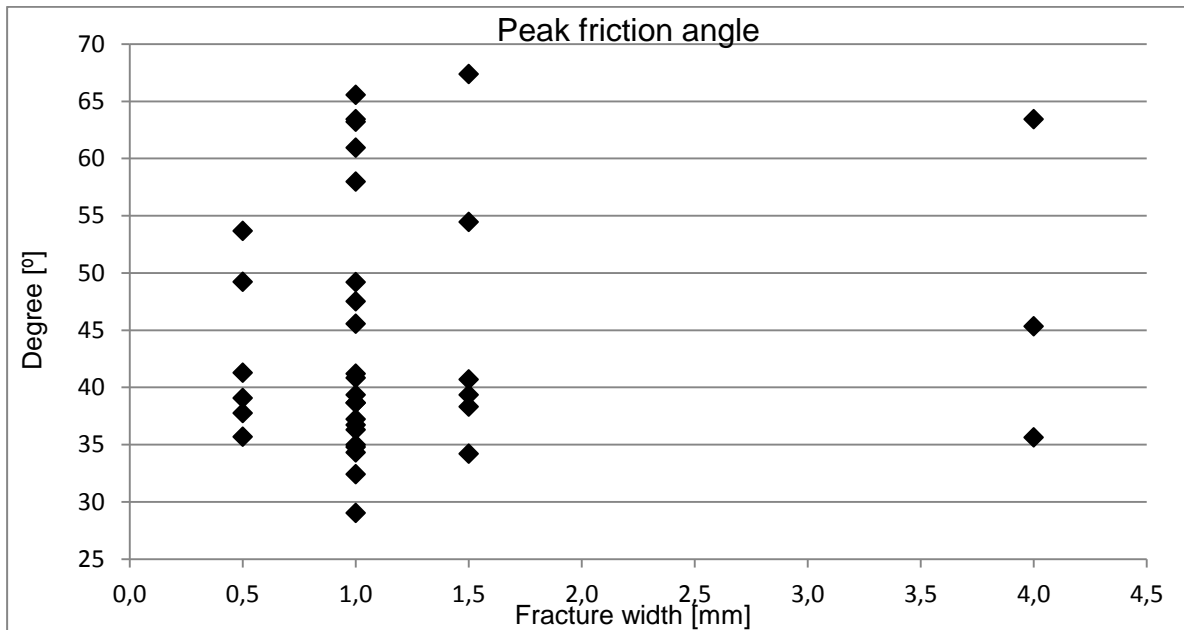


Figure 4.2: The peak friction angle plotted against the fracture width.

In all cases, when the peak friction angle was plotted against the ratio between the normal stress and the uniaxial compressive strength, the peak friction angle is reduced when the stress level increases.

Figure 4.3 indicates that the Young's modulus does not influence the data of the peak friction angle since the data is broadly scattered within each group. However, the ranges of Young's modulus are all narrow which limits the analysis. The peak friction angle is plotted with respect to different ranges of the Young's modulus.

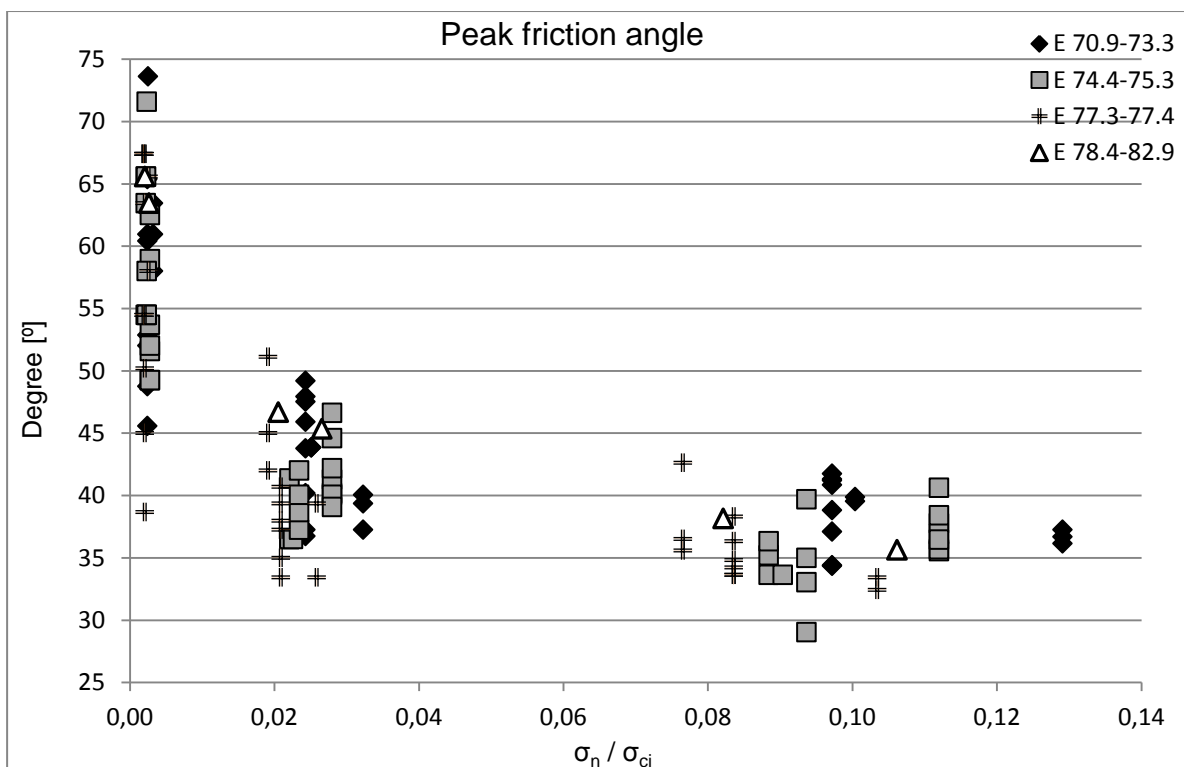


Figure 4.3: The peak friction angle plotted against the ratio between the normal stress and the uniaxial compressive strength, differentiated by ranges of Young's modulus (E , GPa).

Figure 4.4 shows the peak friction angle in relation to the ratio between the normal stress and the uniaxial compressive strength when separated into groups of infilling material and coating mineral. In low stress levels, a slight trend is appearing where the infilling and coating features are detached. However, in higher stresses, the groups are randomly scattered.

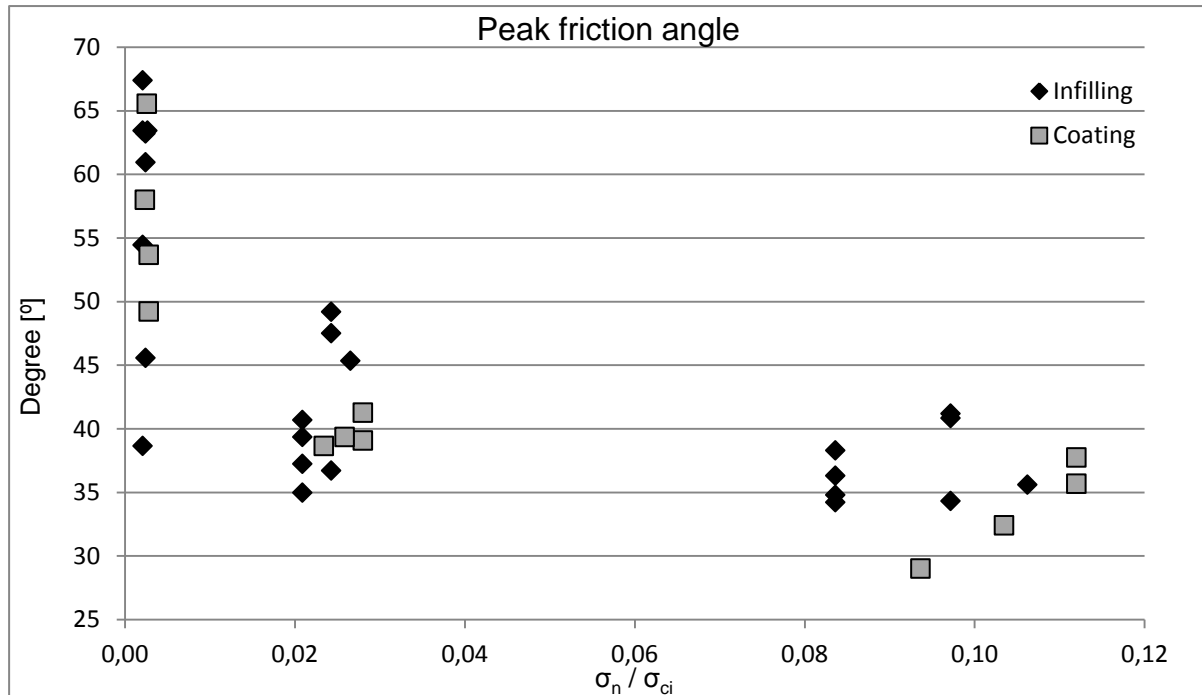


Figure 4.4: The peak friction angle plotted against the ratio between the normal stress and the uniaxial compressive strength, differentiated by groups of infilling material and coating mineral.

Figure 4.5, the peak friction angle is plotted similarly as in Figure 4.4 except that it is sorted into groups of JRC classification. This plot does not reveal any distinguishable patterns.

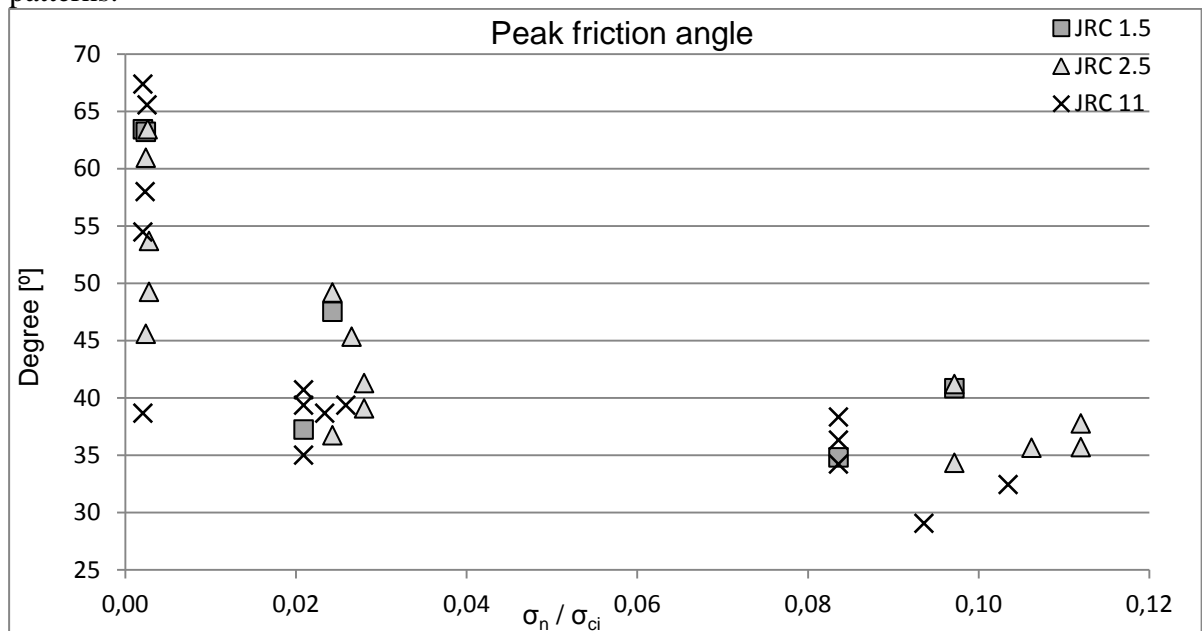


Figure 4.5: The peak friction angle plotted against the ratio between the normal stress and the uniaxial compressive strength, differentiated by JRC number.

Statistical data of the peak friction angle is presented in Table 4.3. The mean value, the standard deviation and the coefficient of variation is calculated for each normal load used during the direct shear tests.

Table 4.3: Mean, standard deviation and coefficient of variation of the peak friction angle.

Peak friction angle, ϕ_p [°]				
Stress level [MPa]	N° of samples	Mean [°]	Standard deviation [°]	Coefficient of variation, %
0.5	41	58.3	7.6	13.1
5	41	41.0	4.2	10.4
20	41	36.6	2.9	7.9

The residual friction angle, derived from the direct shear tests, exhibits similar behaviour as the peak friction angle. No visible patterns or trends have been discovered in relation to the affecting parameters. Figure 4.6 verifies the influence of increasing normal stress of the residual friction angle. The mean of the residual angle is similarly decreasing.

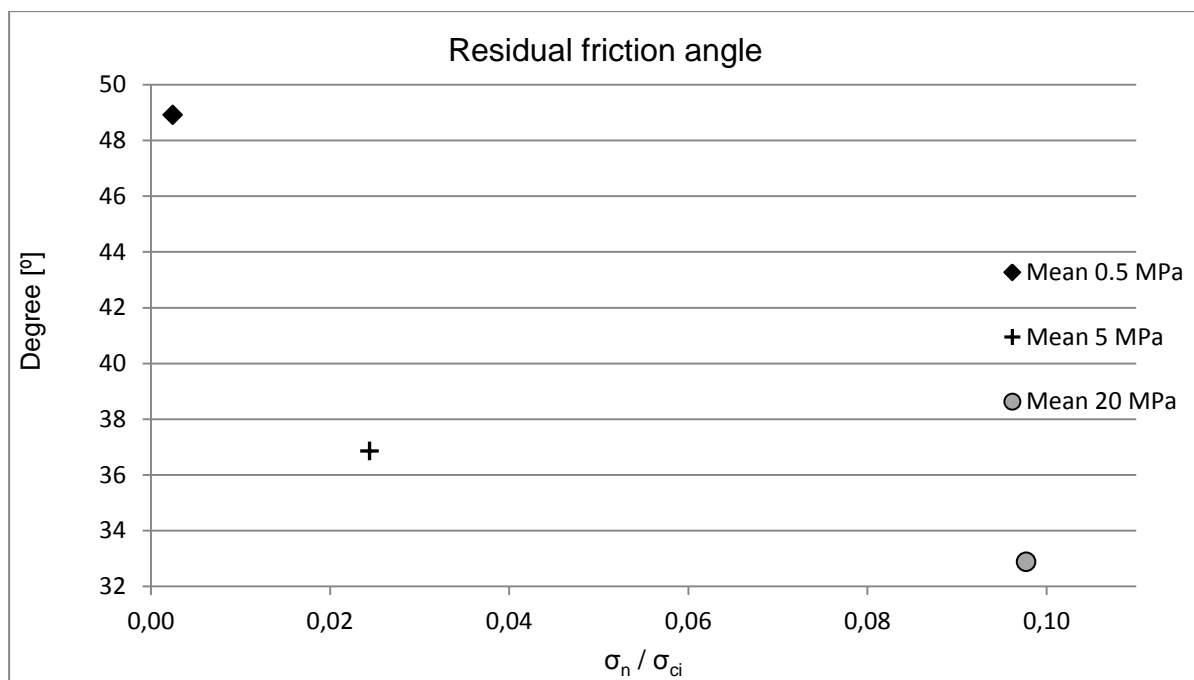


Figure 4.6: The mean value of the residual friction angle for each normal load is plotted against the ratio between the normal stress and the uniaxial compressive strength.

Similarly to the statistical data of the peak friction angle, the mean value, the standard deviation and the coefficient of variation of the residual friction angle is presented in Table 4.4. The data is considered for each normal load used during the direct shear tests.

Table 4.4: Mean, standard deviation and coefficient of variation of the residual friction angle.

Residual friction angle, ϕ_{res} [°]				
Stress level [MPa]	N° of samples	Mean [°]	Standard deviation [°]	Coefficient of variation, %
0.5	41	48.9	4.4	9.1
5	41	36.9	2.9	7.9
20	41	32.9	4.6	13.9

The mean, standard deviation and coefficient of variation of the parameters in the Mohr-Coulomb approach is compiled in Table 4.5.

Table 4.5: Mean value, standard deviation and coefficient of variation of the parameters in the Mohr-Coulomb approach: peak friction angle, residual friction angle, peak cohesion and residual cohesion.

	N° of samples	Mean	Standard deviation	Coefficient of variation [%]
Peak friction angle [°]	41	35.5	2.9	8.3
Residual friction angle [°]	41	32.1	5.0	15.6
Peak cohesion [MPa]	41	0.6	0.3	49.7
Residual cohesion [MPa]	41	0.4	0.3	67.5

4.2.2 Asperity failure component

The basic friction angle has been measured during tilt test. In addition to this, in the same diagram, the difference between the peak friction angle and the dilation angle has been calculated. The reason for this approach is to study the effect from the asperity failure component. Figure 4.7 presents the quantity of the basic friction angle and the difference between the peak friction angle and the dilation angle.

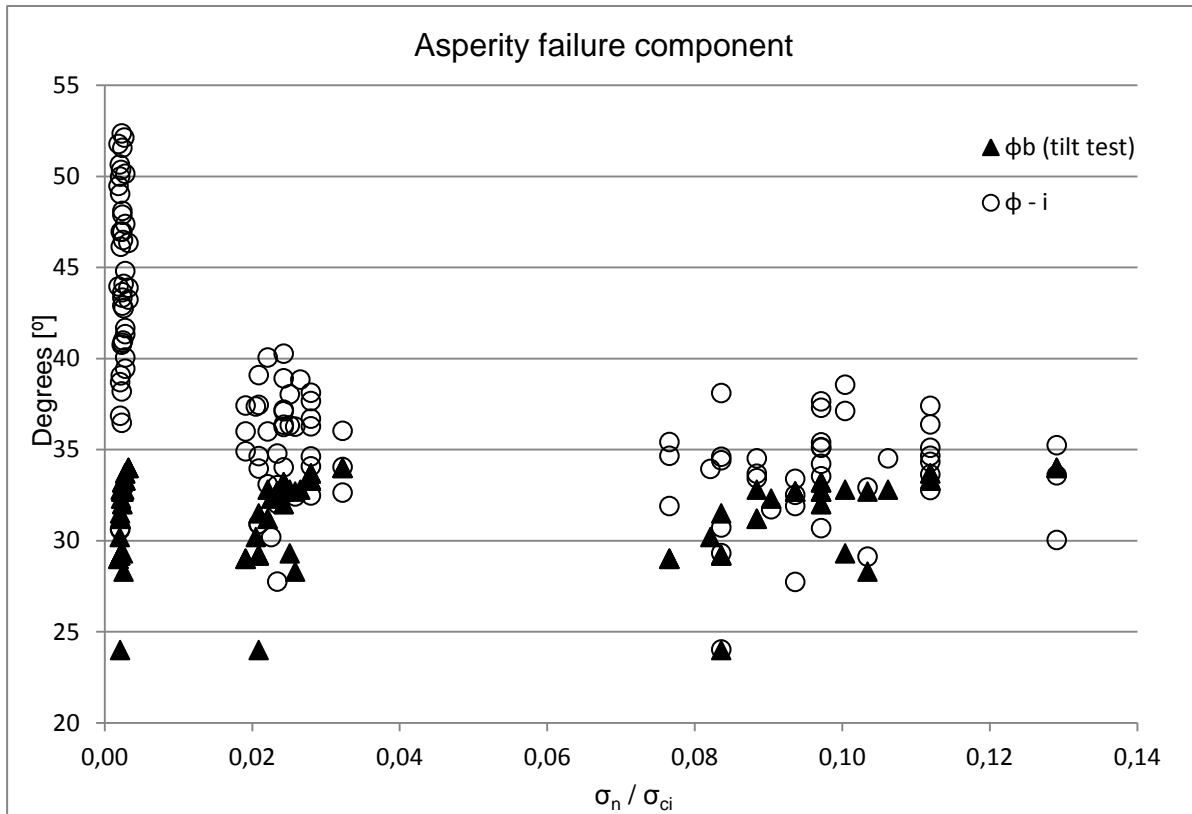


Figure 4.7: The two different basic friction angles plotted against the ratio between the normal stress and the uniaxial compressive strength.

During the stress level of 0.5 MPa, the two basic friction angles are visibly separated. The calculated basic friction angle has a higher mean value than the basic friction angle from tilt testing but approaches the same value as the stress level increases.

4.2.3 Basic friction angle

The basic friction angle does not show the expected trend of increasing with increasing uniaxial compressive strength of the material. On the contrary, the trend decreases. Figure 4.9 does not show any obvious trend between the basic friction angle and the Schmidt rebound number.

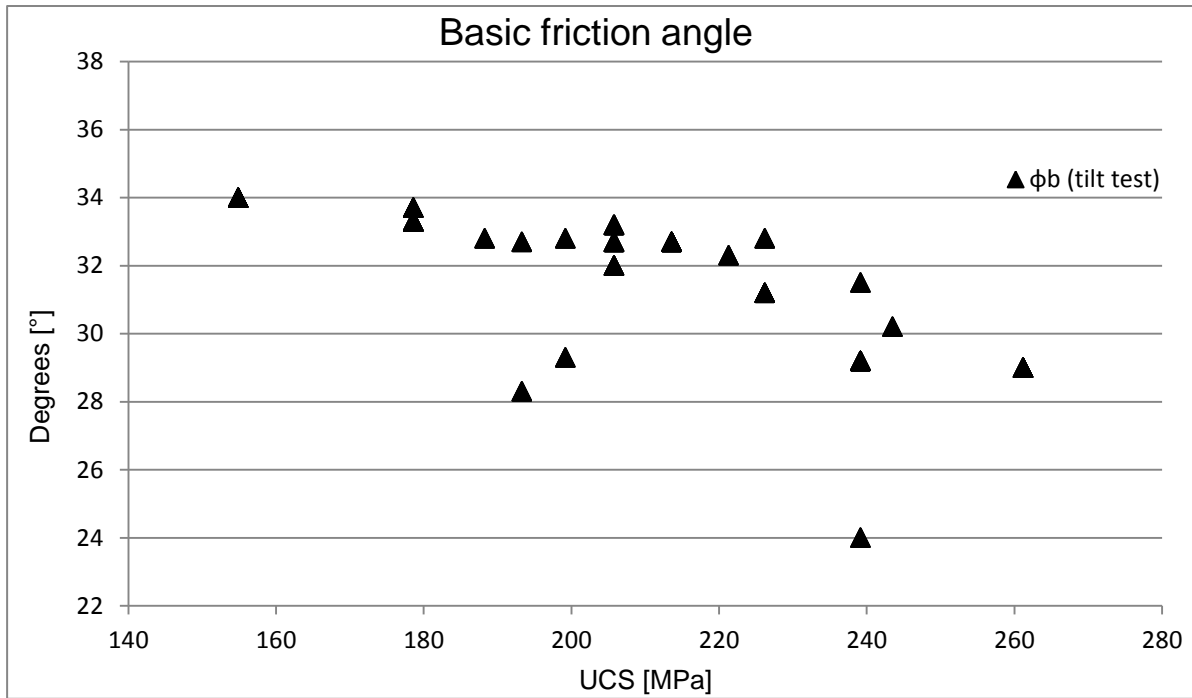


Figure 4.8: The basic friction angle is plotted against the uniaxial compressive strength.

4.2.4 Dilation angle

The analysis of peak dilation angle reflects the same results as found in the analysis of the peak friction angle. The peak dilation angle decreases as the stress level grows and the plot does not show any apparent signs of JRC or fracture width influences (Figure 4.10 and Figure 4.11).

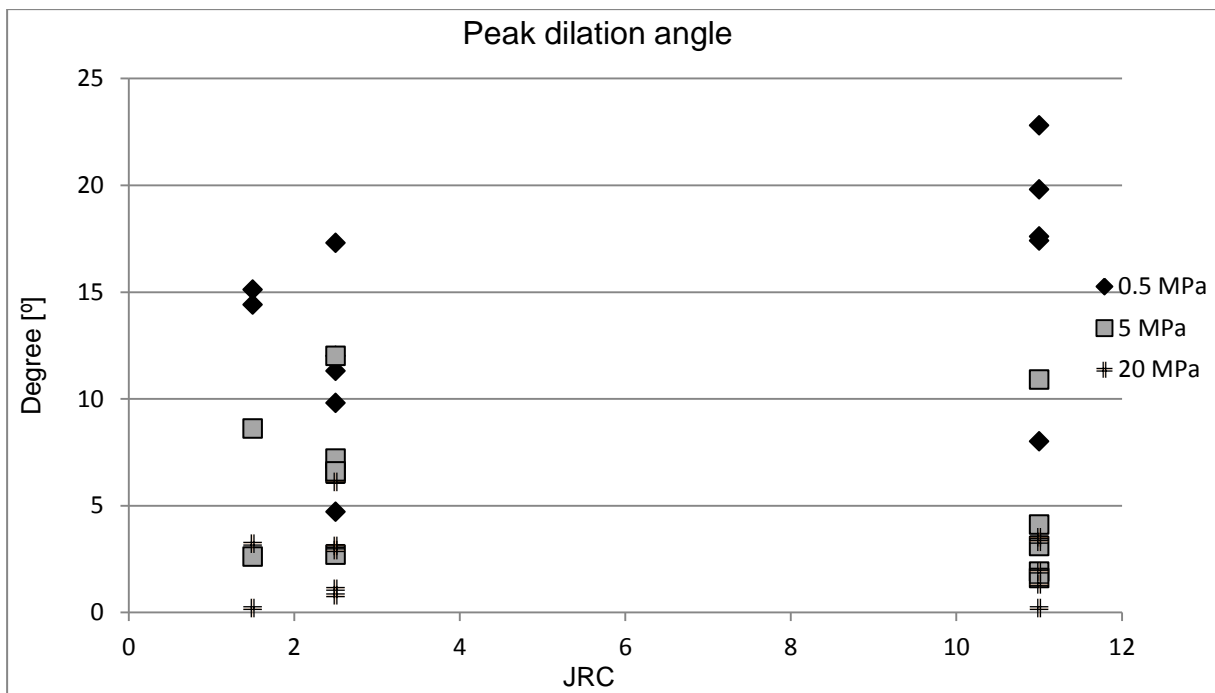


Figure 4.10: The peak dilation angle plotted against JRC, differentiated by groups of normal load.

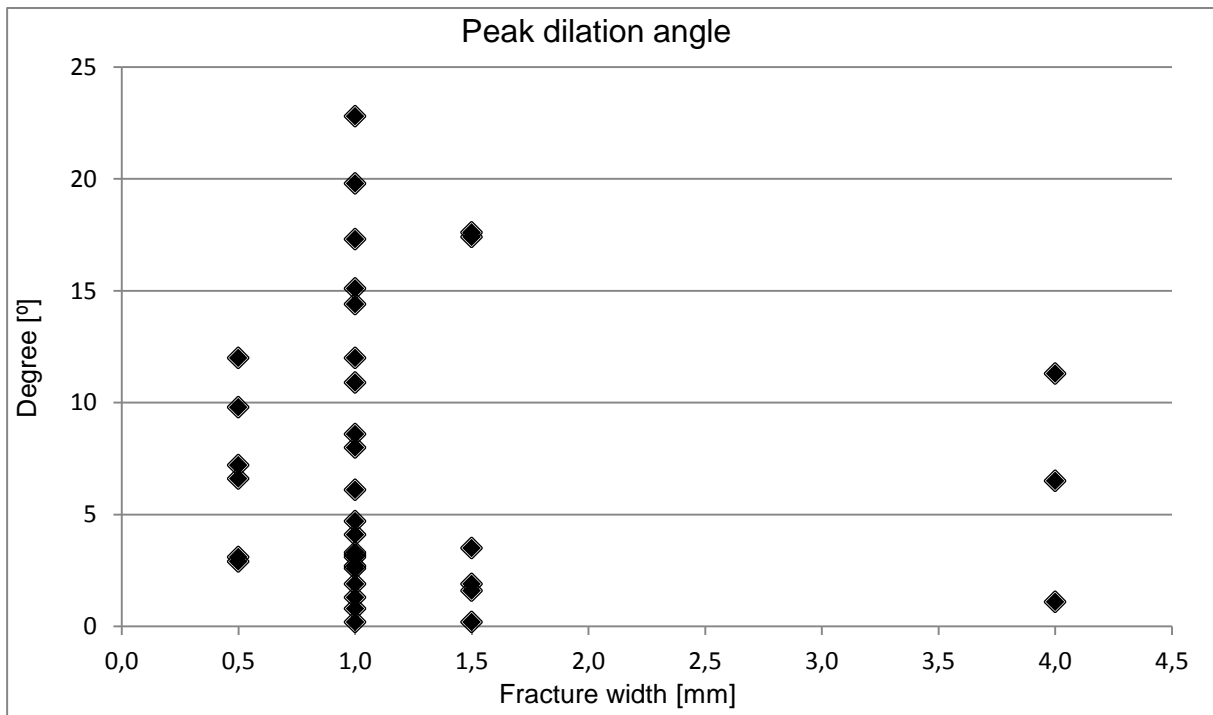


Figure 4.11: The peak dilation angle plotted against the fracture width.

In Figure 4.12, the peak dilation angle is differentiated by different groups of the Young's modulus and plotted against the ratio between the normal stress and the uniaxial compressive strength. Analogously to the peak friction angle, no clear relations could be distinguished.

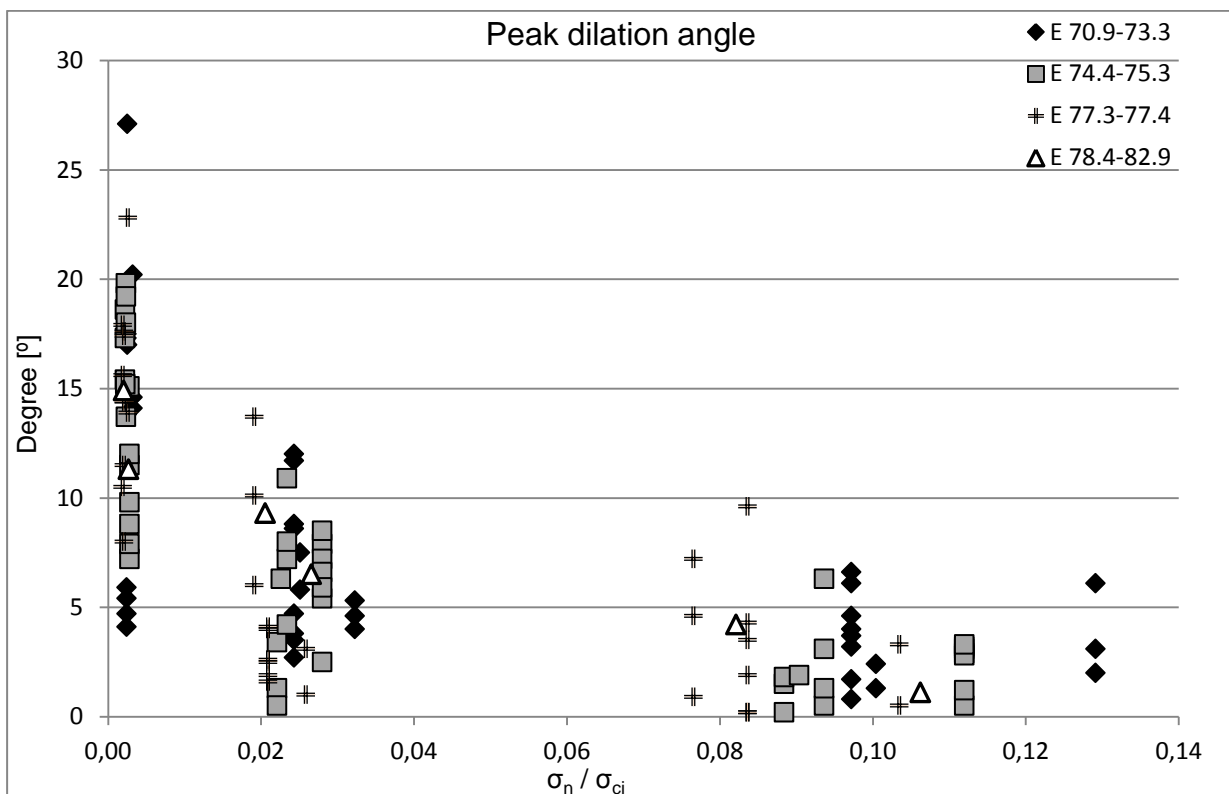


Figure 4.12: The peak dilation angle is plotted against the ratio between the normal stress and the uniaxial compressive strength, differentiated by groups of the Young's modulus (E , GPa).

Figure 4.13 returns a comparable appearance as the similar plot of the peak friction angle, where coating gives slightly higher angle values at low stress. For high normal stresses, no trend caused by the infilling characteristics could be detected since the data is randomly scattered.

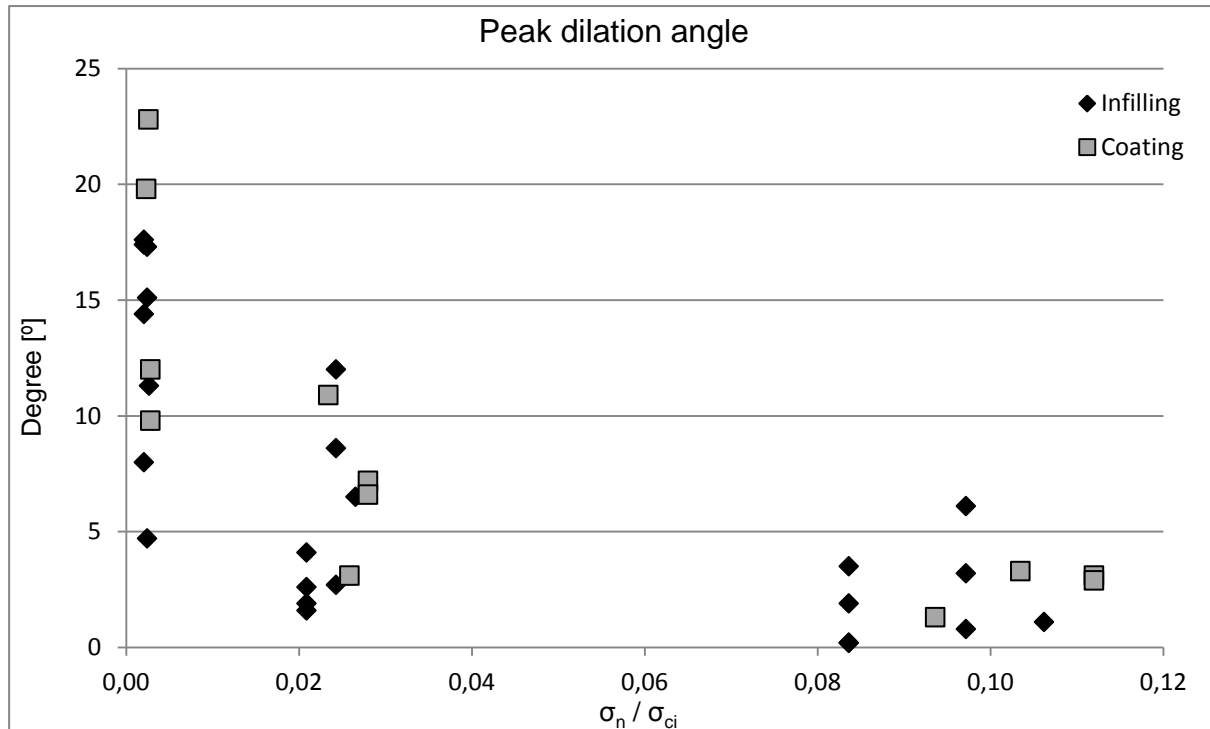


Figure 4.13: The peak dilation angle according to infilling characteristics plotted against the ratio between normal stress and uniaxial compressive strength.

In Table 4.6, the mean value, the standard deviation and the coefficient of variation of the peak dilation angle is presented. The statistical data is divided into groups of the normal stress used during the direct shear tests.

Table 4.6: Mean, standard deviation and coefficient of variation of the peak dilation angle.

Peak dilation angle, i [°]				
Stress level [MPa]	N° of samples	Mean [°]	Standard deviation [°]	Coefficient of variation, %
0.5	41	14.1	4.9	35.2
5	41	5.7	3.2	55.6
20	41	2.9	2.1	72.7

The succeeding plot, Figure 4.14, contains a comparison between the asperity failure component and the peak dilation angle when exposed to increasing normal stress. Both of them decrease with approximately equal rate.

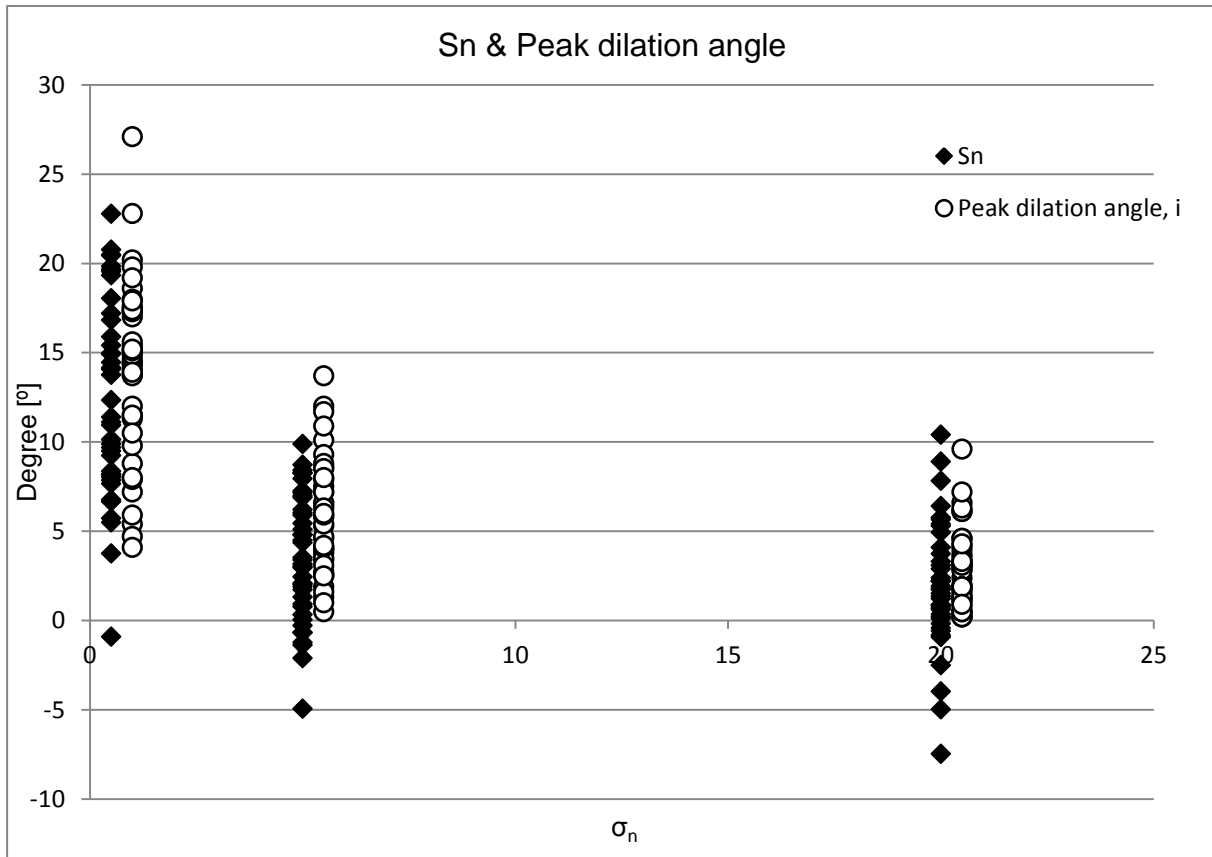


Figure 4.14: The asperity failure component and dilation angle plotted against the normal stress. The asperity failure component is calculated according to the following equation: $s_n = \theta_{tot} - (\theta_b + i)$.

4.2.5 Normal and shear stiffness

The normal stiffness has the same quantity regardless the normal stress used in the direct shear test, given that it was determined through another test. The shear stiffness has however been differentiated by normal stress.

The plot of the normal stiffness and shear stiffness to the JRC, Figure 4.15 and Figure 4.6, do not bring any clear results where trends or patterns can be distinguished. The JRC values are scattered when plotted against the shear stiffness and the groups of normal loads can be found at all different JRC values. However, it is clear that the shear stiffness is increasing with higher normal stress.

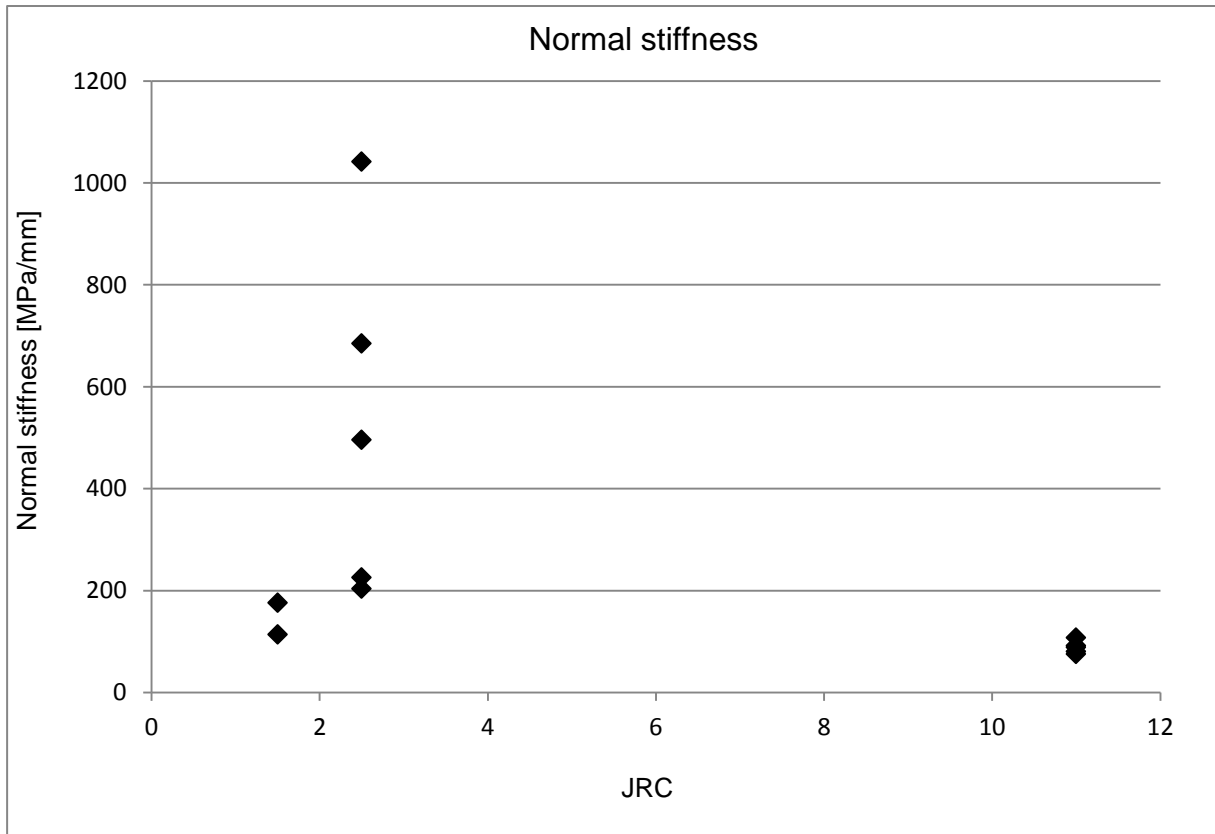


Figure 4.15: The normal stiffness against the JRC.

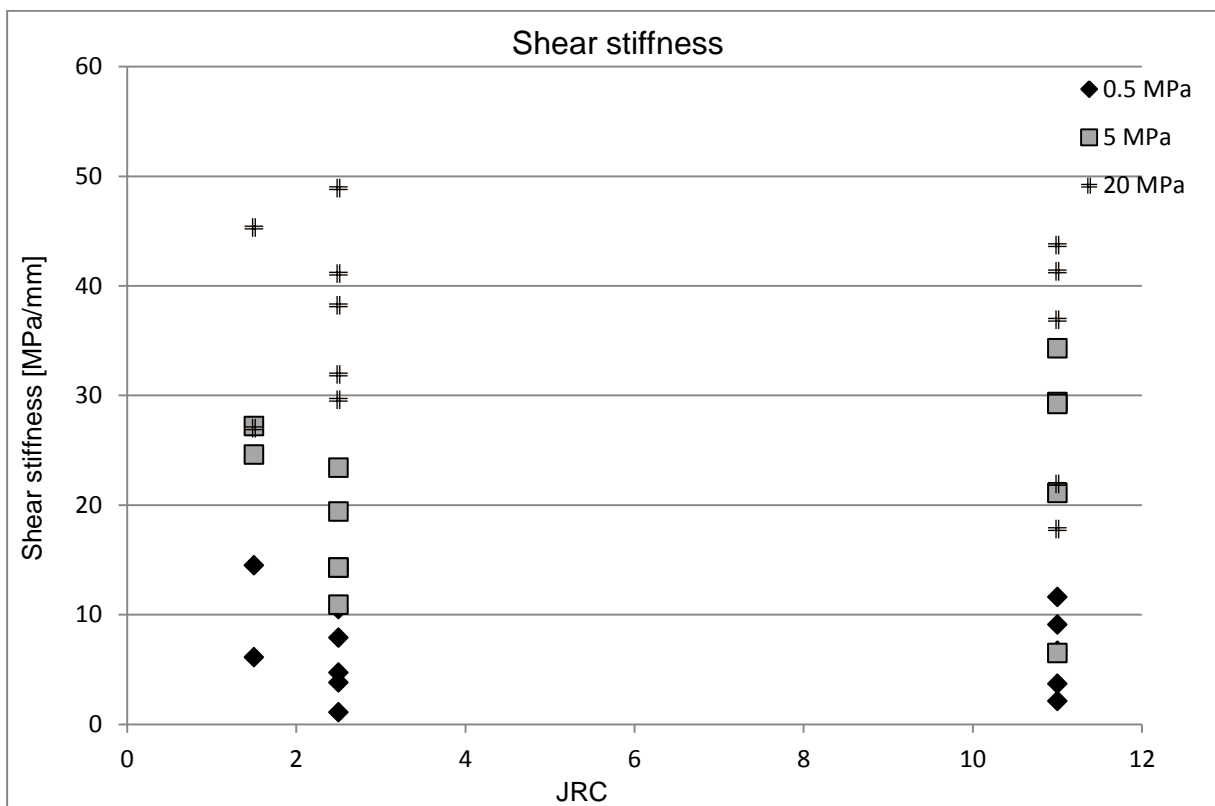


Figure 4.16: The shear stiffness against the JRC, differentiated by the groups of the normal stress.

In Figure 4.17 and Figure 4.18, the normal and shear stiffness are plotted against the fracture width with respect to the infilling characteristics. The analysis is limited by the few data points of fracture widths larger than 1 millimetre. No trends can be established since the infilling and coating points are more or less equally scattered over the quantity of stiffness. The infilling material is more presented in the wider fractures, which is expected.

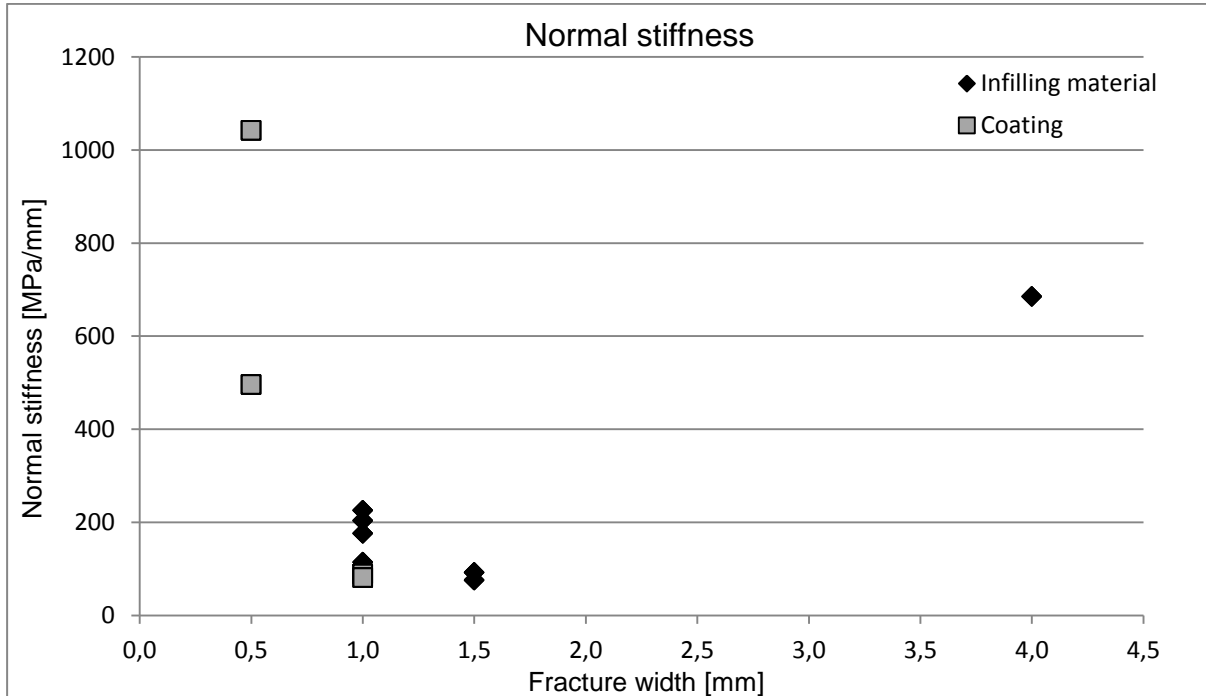


Figure 4.17: The normal stiffness against the fracture width, differentiated by infilling characteristics.

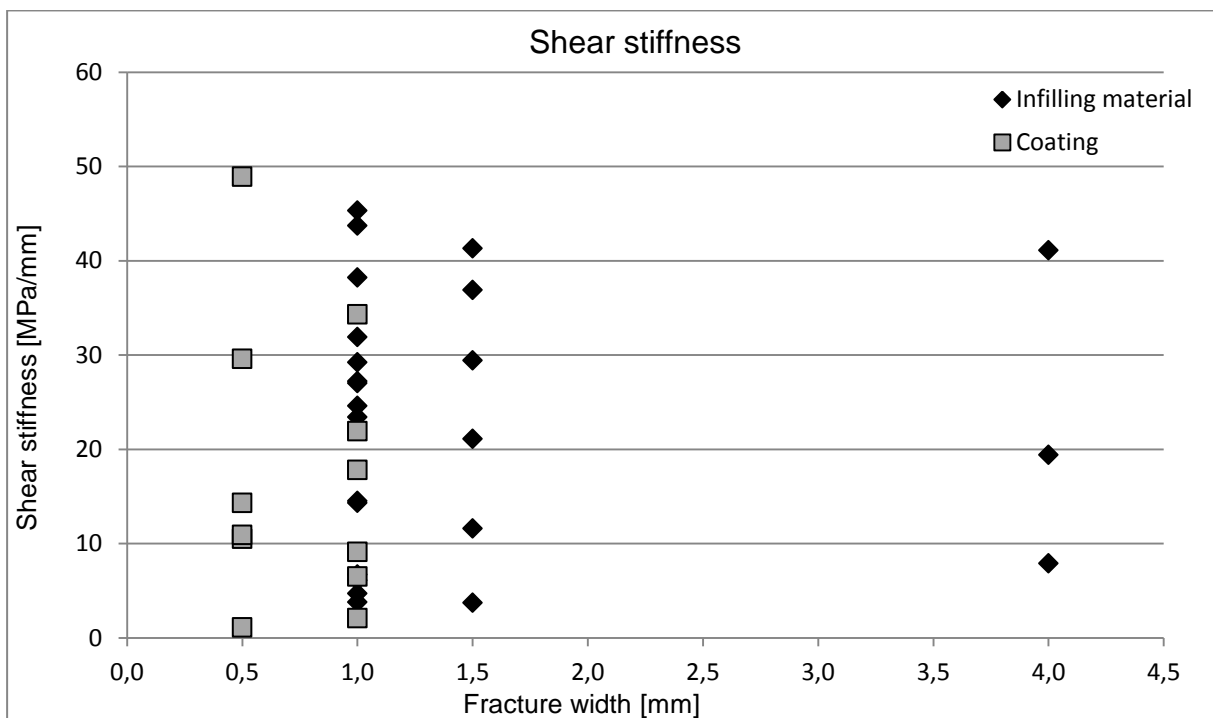


Figure 4.18: The shear stiffness against the fracture width, differentiated by infilling characteristics.

Figure 4.19 and Figure 4.20 show that the Young's modulus has no apparent influence on the normal and shear stiffness, according to this data. The shear stiffness increases with higher normal load.

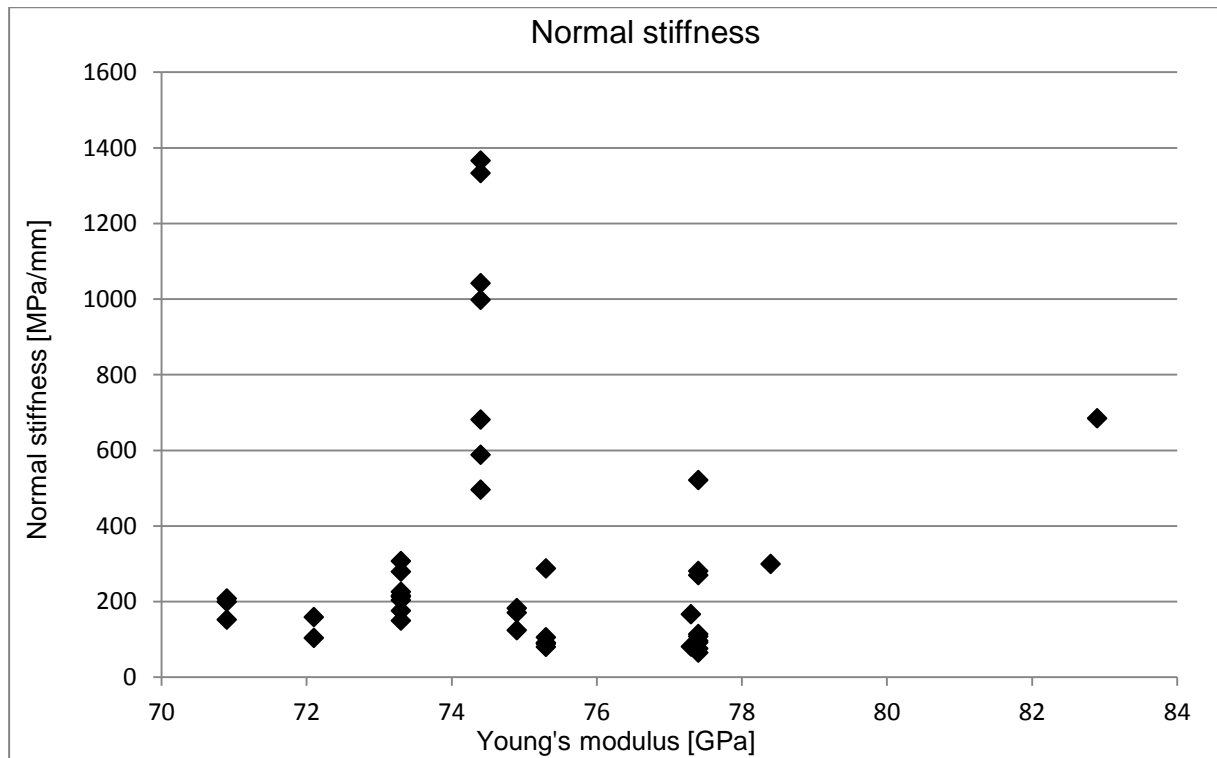


Figure 4.19: The normal stiffness plotted against the Young's modulus.

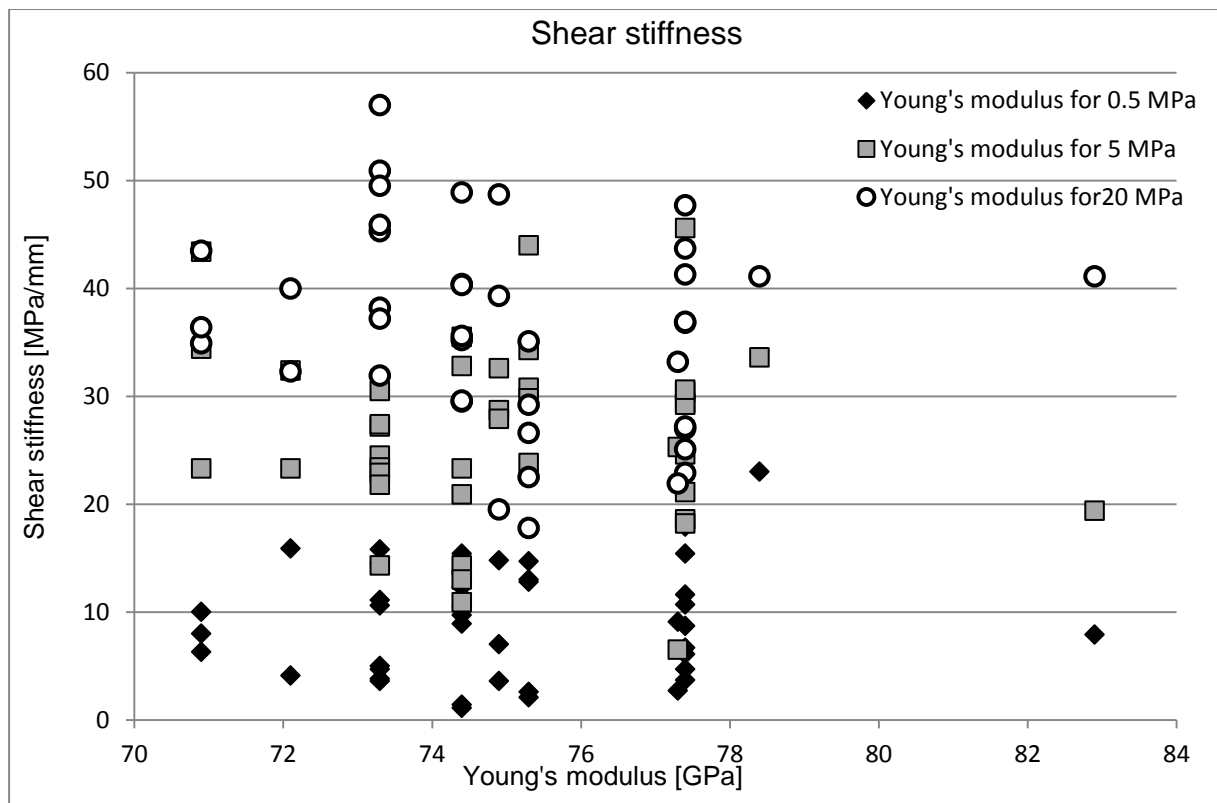


Figure 4.20: The shear stiffness plotted against the Young's modulus, differentiated by groups of normal stress.

The statistical data for the normal and shear stiffness is presented in Table 4. and Table 4.8. It includes the mean value, the standard deviation and the coefficient of variation. The data is divided into groups of the normal load used during the direct shear tests for the shear stiffness.

Table 4.7: Mean, standard deviation and coefficient of variation of the normal stiffness.

Normal stiffness, K_n			
N° of samples	Mean [MPa/mm]	Standard deviation [MPa/mm]	Coefficient of variation, %
41	319.2	328.4	102.9

Table 4.8: Mean, standard deviation and coefficient of variation of the shear stiffness.

Shear stiffness, K_s				
Stress level [MPa]	N° of samples	Mean [MPa/mm]	Standard deviation [MPa/mm]	Coefficient of variation, %
0.5	41	9.1	5.1	56.5
5	41	26.4	8.4	31.7
20	41	36.3	9.2	25.3

5 Discussion

The main purpose of this study was to investigate the possibilities of predicting the peak shear strength of rock fractures out of the affecting parameters. The study produced a data compilation of 41 rock fractures containing information from shear, tilt and uniaxial compressive strength testing as well as field mapping.

The study returned a number of interesting observations during the evaluation of the interaction matrix and the influence analysis. The interaction matrix predicted the probable relationships between mechanical and affecting parameters. A ratio between the uniaxial compressive strength and the effective normal stress reflected the contact area between the fracture walls. The UCS of the data had not much variation so when the contact area increased it depended on greater effective normal stress. The results supported the interaction matrix forecasts provoked by increased effective normal stress; the friction and dilation angles decreased and the normal and shear stiffness increased.

Increased roughness and aperture did not have the same expected outcome. The results were scattered randomly for all mechanical properties. From previous studies, it is clear that the JRC plays a significant role to the shear strength of a rock fracture. There are two possible explanations for the odd result that the JRC effect could not be observed. The first explanation is that the fractures are so mismatched that the impact of the roughness component is insignificant. This motivates a regularly registration of the fracture matching coefficient. It may be pointless to estimate the JRC from field mapping when the JMC is great, since the JRC loses influence.

The other explanation questions the field mapping of the JRC of bore cores due to the small scale. The bore cores are approximately 5 centimetres in diameter (Jacobsson, 2005), and the large scale waviness component of the JRC can therefore be difficult to detect. To obtain reliable results, the JRC could exclusively be mapped in large scale during field visits.

Considering the effects of increasing scale on the mechanical properties, it is not possible to verify the predictions from the interaction matrix. All laboratory tests were performed on similar sample size.

Infilling materials are expected to weaken the fracture strength in low stress; however, this was not observable in Figure 4.4. The peak friction angle is not distinctively separated by infilling characteristics. Yet, the number of data points was limited. In higher stresses, the infilling characteristics are doubtlessly scattered and seems to have an insignificant impact. To investigate whether the infilling characteristics are relevant in civil engineering and open pit excavations, this study suggests performing similar analyses with more data points.

Regarding the Young's modulus, the influence analysis did not show any trends or patterns. The range was probably too narrow to reveal diverse behaviour (70.9-82.9 GPa).

The asperity failure component is observed in Figure 4.7. The difference between the two series (the basic friction angle from tilt testing and the peak friction angle minus the dilation angle) reflects the asperity failure component. The dilation angle decreases due to increasing normal stress. Yet, the asperity failure component also reduces with increasing

normal stress and the two series convert to a similar value. This means that another roughness component is hidden in the difference between the peak friction angle and the dilation angle, i.e. the asperity failure component, see equation 2.3. Since the asperity failure component is part of the roughness, it is most probably affected by the scale effect (chapter 2.3.5). The basic friction angle from tilt testing is however more or less constant and agrees with the calculated basic friction angle at higher stresses. This can be useful for deep mining projects: at large stress conditions, the basic friction angle can be picked directly from the tilt test.

Furthermore, it appeared that the asperity failure component was of the same magnitude as the dilation angle. The ratio between the asperity failure component and the dilation angle was kept constant for all levels of normal stresses. However, studies by Ladanyi and Archambault (1970) and Barton and Choubey (1977) suggested that this ratio is dependent on the normal stress.

The use of the basic friction angle and the estimated residual friction angle (see equation 2.4) need to be discussed. The data compilation comprises the Schmidt rebound number for both wet and dry surfaces, j and J respectively. The ratio j/J ranges between 1/1.9 and 1/1.2. This gives a difference in angles of approximately 6 degrees. In the study of Barton and Choubey (1977) the basic friction angles of fine-grained granite differ 3 degrees between wet and dry surfaces. The same ratio for coarse-grained granite is 1 degree. This indicates that the influence from weathering is between 3 to 1 degrees, which equals the possible error in this study's analyses that involve the basic friction angle. The error is however impossible to avoid since the direct shear tests are performed on dry samples. A flawless comparison should include the estimated residual friction angle from equation 2.4 together with direct shear test results on wet drill cores.

In addition, the Schmidt rebound number does not correspond to the core logging estimations of the weathering conditions of the rock fracture. It is probably more reliable to use the Schmidt rebound hammer (correctly calibrated) than to rely on subjective estimations during the core logging of the fractures. This is another indication to reconsider both procedures and utility of field mapping and core logging.

The data of this thesis did not show an increasing trend of the basic friction angle in relation to increasing uniaxial compressive strength. The range of the uniaxial compressive strength is however not wide enough to produce a fully reliable result. The material is mostly granitic rock. A similar comparison but with numerous rock types would be more consistent.

Table 5.1 summarises the mean values of the peak friction angle, the residual friction angle and the peak dilation angle from the direct shear tests at 20 MPa, when the shear strength is defined as the secant between the shear and normal stress.

Table 5.1: Mean value of the peak friction angle, the residual friction angle and the peak dilation angle at 20 MPa.

Mechanical property	Mean (deep mining, 20 MPa)
Peak friction angle [°]	36.6
Residual friction angle [°]	32.9
Peak dilation angle [°]	2.9

Hoek et al. (2005) suggested a method that derives representative values of cohesion and peak friction angle from the slightly curved failure envelop. They propose using Barton's

equation (1973) when the failure envelope is still arched. Later, when the curve is straighter, the fitting is estimated with peak friction angle and peak cohesion. Assuming an average effective normal stress of 10 MPa and 20 MPa, the values they calculated for the peak friction angle and the peak cohesion correspond surprisingly well with the data of this study, see Table 5.2.

Table 5.2: Comparison of peak friction angle and peak cohesion between the data of this study and the values calculated by using the equations suggested by Hoek et al. (2005).

	Hoeak et al. (2005)		Data from Table 4.5	
	ϕ_p	c_p	ϕ_p	c_p
10 MPa	36,3	0,7	35,5	0,6
20 MPa	34,7	1,3		

As previous studies show that the scale effect is significant in low stress conditions, mechanical properties developed from laboratory sized samples are not reliable parameters for stability analyses. This study can therefore not offer guidelines for civil engineering or open pit rock projects.

However, the study suggests using the secant friction angle instead of the Mohr-Coulomb approximation in civil engineering, if the scale effect is accounted for. It reflects the peak shear strength of the rock fracture at a specific stress level without involving the cohesion. Cohesion is a mathematical invention to approximate several values to the best fitting of a straight line. The shear strength is thus approximated as a mean value of different stress levels. If the actual stress level in an engineering project can be estimated, there is no good reason to select mean shear strength of the rock fractures, since it also can overestimate the strength at low stress levels.

Concerning the normal stiffness, the data was extensively scattered and as a result, with a large standard deviation. A fully mated fracture would expectably exhibit a large normal stiffness. Since the fracture matching coefficient is not recorded, it is however not possible to draw any conclusions from the results.

The shear stiffness has a more united result. Yet, the shear stiffness is also subject to a considerable scale effect and the laboratory developed data of this study cannot offer reliable guidelines.

The study has found out that it is possible to give guidelines for some of the mechanical properties for rock fractures in granitic rock masses with open and fresh to moderately altered fractures.

The data compilation serves as a helpful tool to further research, comprising important and numerous parameters. Furthermore, the study generated another important tool for the understanding the relationship between the mechanical properties and affecting parameters of rock fractures: the interaction matrix.

6 Conclusions

6.1 General conclusions

This study has showed that it is possible to use mapping and core logging data, for example JRC, JCS and tilt tests to estimate with reasonable approximation the shear strength of joints in deep environments (under high normal stress).

The study offers an estimate of the cohesion and friction angle for deep mining industry according to the Mohr-Coulomb constitutive model based on results of direct shear tests on fracture samples, see Table 6.1. The method of Hoek et al. (2005) where the Mohr-Coulomb friction angle and cohesion are approximated based on parameters that can be measured on the field (JRC, JCS and basic friction angles) are close to the values in Table 6.1, see Table 5.2. Recall that this comparison merely concern fractures in granitic rock, provided that the fractures are open and relatively fresh.

Table 6.1: The Mohr-Coulomb approximation of the peak friction angle and the peak cohesion based on direct shear fracture shear tests results at 0.5 MPa, 5 MPa and 20 MPa normal stress.

Data from Table 4.5	ϕ_p	c_p
10 MPa	35,5	0,6
20 MPa		

Table 6.2 summarises the mean values of the friction angles at 20 MPa, when the shear strength is defined as the secant between the shear and normal stress. Note that the value of the peak friction angle at this normal stress level is also close to the one estimated using the Mohr-Coulomb constitutive model, see Table 6.1.

Table 6.2: Mean values of friction angles for deep mining projects, defined as the secant between the shear and normal stress at 20 MPa normal stress.

Mechanical property	Mean (20 MPa)
Peak friction angle [°]	36.6
Residual friction angle [°]	32.9
Peak dilation angle [°]	2.9

Moreover, the study resulted in a data compilation and an interaction model that serve further analyses and studies in the field of rock mechanics.

6.2 Suggestions for future research

This study did not cover the scale effect. However, it is known from previous studies that scale has a significant impact on the mechanical properties of the fracture. A research on the scale effect of rock fractures would be useful in order to understand the phenomenon better. This is especially important for civil engineering projects that are subject to scale problems in a larger extent than deep mining.

The results concerning the ratio of the asperity failure component and the dilation angle at different stress levels are interesting. Further research into this area is needed.

The study also suggests additional compiling of data, including the fracture matching coefficient and different rock types, in order to continue analyses of the mechanical behaviour of rock fractures.

The field mapping and core logging of the JRC were questioned in this study due to the scale effect. An agreement between characterization and shear tests is both necessary and pressing.

Bibliography

Alejano, L.R., Alonso, E., 2005. Considerations of the dilatancy angle in rocks and rock masses. *International Journal of Rock Mechanics & Mining Science*, Vol. 42, pp. 481-507.

Bandis, S.C., Lumsden, A.C., Barton, N.R., 1983. Fundamentals of Rock Fracture Deformation. *International Journal of Rock Mechanics & Mining Science*, Vol. 20, pp. 249-268.

Barton, N.R., 1973. Review of a new shear-strength criterion for rock fractures. *Engineering geology*, Vol. 7, Nr. 4, pp. 287-332.

Barton, N.R., Choubey, V., 1977. The shear strength of rock fractures in theory and practice. *Rock Mechanics*, Vol. 10, pp. 1-54.

Barton, N.R., 1981. Estimation of in-situ fracture properties, Näsliden mine. *Appl. Rock Mech., Mining Proc., Conf.* Luleå, Sweden

Barton, N.R. 1987. *Rock mass Classification and Tunnel Reinforcement Selection using the Q-system*. Proc. ASTM Symp.on Rock Classification Systems for engineering Purposes, Cincinnati, Ohio.

Barton, N.R., Bandis, S., 1982. *Effects of block size on the shear behaviour of fractured rock*. 23rd US Symposium on Rock Mechanics, Berkeley, CA, pp. 739-60.

Borri-Brunetto, M., Carpinteri, A., Chiaia, B., 1998. Scaling phenomena due to fractal contact in concrete and rock fractures. *International Journal of Fracture*, Vol. 95, pp. 221-238.

Brown, E.T., 1981. Rock characterization testing & monitoring: ISRM Suggested Methods. Commission on testing methods, international society for rock mechanics, Pergamon Press.

Chryssanthakis, P., 2003. *Results of tilt testing*. Report: SKB P-03-108. Forsmark site investigation.

Hoek, E., 2007. *Practical rock engineering*.

Hoek E., Kaiser P.K., Bawden W.F., 2005. *Support of underground excavations in hard rock*. Fourth Edition, pp. 55.

Hopkins, D.L., 2000. The implication of fracture deformation in analyzing the properties and behaviour of fractured rock masses, underground excavations, and faults. *International Journal of Rock Mechanics & Mining Science*. Vol. 37, pp.175-202.

- Goodman, R.E., Talyor R.L., Brekke T.L., 1968. A model for the mechanics of fractured rock. *Journal of the Soil Mechanics and Foundations Division*, Vol. 94, pp. 637-660.
- Goodman, R.E., 1989. *Introduction to Rock Mechanics*. John Wiley & Sons.
- Jacobsson, L., 2004. *Uniaxial compression test of intact rock*. Report: SKB P-04-223. Forsmark site investigation.
- Jacobsson, L., 2005. *Normal loading and shear tests on fractures*. Report: SKB P-05-08. Forsmark site investigation.
- Johansson, F., 2003. *Stability Analyses of Large Structures Founded on Rock - An Introductory Study*. Licentiate Thesis, Royal Institute of Technology, Stockholm
- Johansson, F., 2009. *Shear strength of unfilled and rough rock fractures in sliding stability analysis of concrete dams*. Doctoral thesis, Royal Institute of Technology, Stockholm.
- Ladanyi, B., Archambault, G., 1970. Simulation of the shear behaviour of a fractured rock mass. Proceedings of the 11th U.S. Symposium on Rock Mechanics, Vol. 7, pp. 105-125.
- Marache, A., Riss, J., Gentier, S., 2008. Experimental and modeled behaviour of a rock fracture under normal stress. *Rock Mechanics and Rock Engineering*, Vol. 41, pp.869-892.
- Fardin, N., 2003. *The effect of scale on the morphology, mechanics and transmissivity of single rock fractures*. Doctoral thesis, Royal Institute of Technology, Stockholm.
- Seidel, J.P., Haberfield, C.M., 1995. Towards an understanding of fracture roughness. *Rock mechanics and Rock Engineering*, Vol. 28, pp. 69-92.
- Wines, D.R., Lilly, P.A., 2003. Estimates of rock shear strength in part of the Fimiston open pit operation in Western Australia. *International Journal of Rock Mechanics & Mining Science*. Vol. 40, pp. 929-937.
- Woo, I., Fleurisson, J., Park, H., 2010. Influence of weathering on shear strength of fractures in a porphyritic granite rock mass in Jechon area, South Korea. *Geoscience journal*. Vol. 14, pp. 289-299.
- Yoshinaka, R., Yoshida, J., Arai, H., Arisaka, S., 1993. Scale effects on shear strength and deformability of rock fractures. *Scale Effects in Rock Masses*. Vol. 93, pp. 143-149.
- Zangerl, C., Evans, K.F., Eberhardt, E., Loew, S., 2008. Normal stiffness of fracture in granitic rock: A compilation of laboratory and in-situ experiments. *International Journal of Rock Mechanics & Mining Sciences*, Vol. 45, pp. 1500-1507.
- Zhao, J., 1997. Fracture surface matching and shear strength (Part A: fracture matching coefficient (JMC). Part B: JRC-JMC Shear Strength Criterion). *International Journal of Rock Mechanics and Mining Sciences*, Vol. 34, pp. 173-185.

Appendix A

Appendix A presents statistical data and plots based on all data in the data compilation. The statistical data of the mechanical and affecting parameters is found in Table A.

Table A: Mean and standard deviation for mechanical and affecting parameters, all data included.

Parameters	Mean	Standard deviation
$\phi_{p0.5}$ [°]	58.3	7.6
ϕ_{p5} [°]	41.0	4.2
ϕ_{p20} [°]	36.6	2.9
$\phi_{res0.5}$ [°]	48.9	4.4
ϕ_{res5} [°]	36.9	2.9
ϕ_{res20} [°]	32.9	4.6
ϕ_b [°]	31.7	2.1
$i_{0.5}$ [°]	14.1	4.9
i_5 [°]	5.7	3.2
i_{20} [°]	2.9	2.1
K_n [MPa/mm]	319.2	328.4
$K_{s0.5}$ [MPa/mm]	9.1	5.1
K_{s5} [MPa/mm]	26.4	8.4
K_{s20} [MPa/mm]	36.3	9.2
JRC	5.6	5.3
JCS (Barton, 1973) [MPa]	190.4	36.5
Schmidt rock rebound number, J (dry)	48.2	2.4
Schmidt fracture rebound number, j (wet)	36.4	4.8
σ_{ci} [MPa]	208.6	28.1

Different plots of the peak friction angle are shown in Figure A, Figure B, Figure C and Figure D. Figure A displays how the peak friction angle is not obviously related to the JRC values of this data compilation.

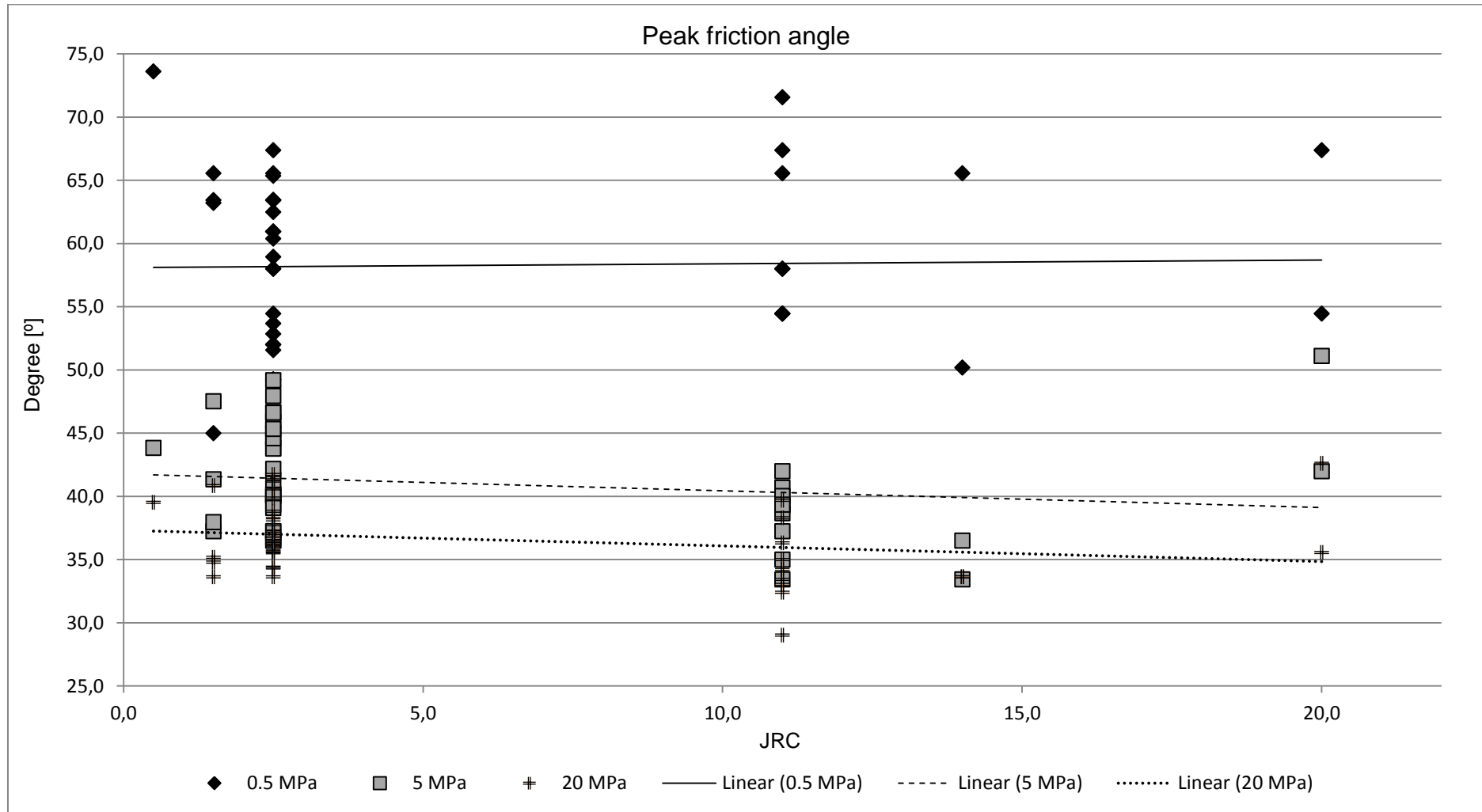


Figure A: The peak friction angle is plotted against the JRC according to normal load used during the direct shear test.

The peak friction angle seems to decrease with larger fracture width in Figure B when comparing the 0.5 and 1 millimetres opening.

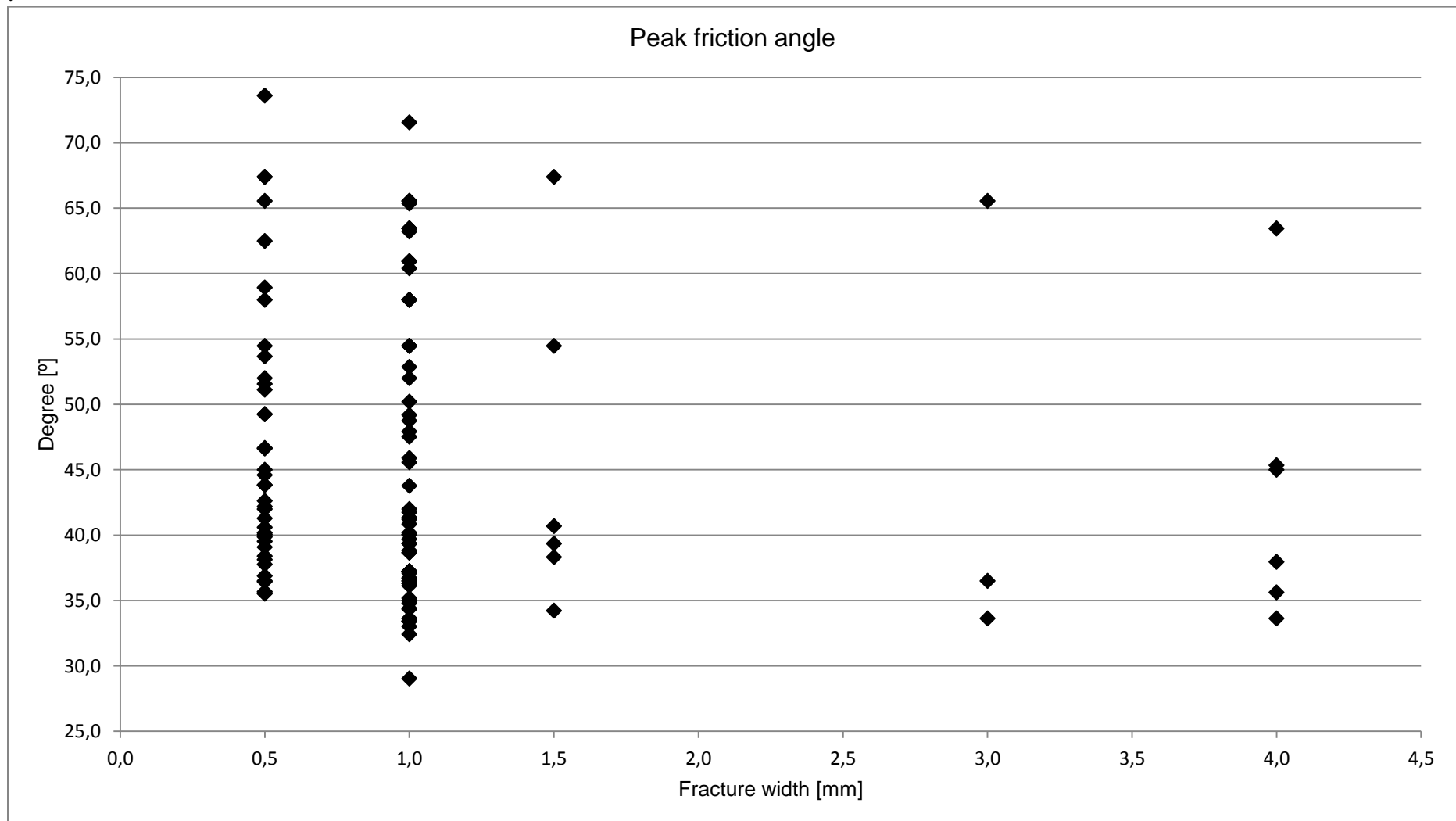


Figure B: The peak friction angle is plotted against the fracture width.

In Figure C, the peak friction decreases with higher normal load. In low stress condition, the infilling characteristics seem to matter more than at high stresses.

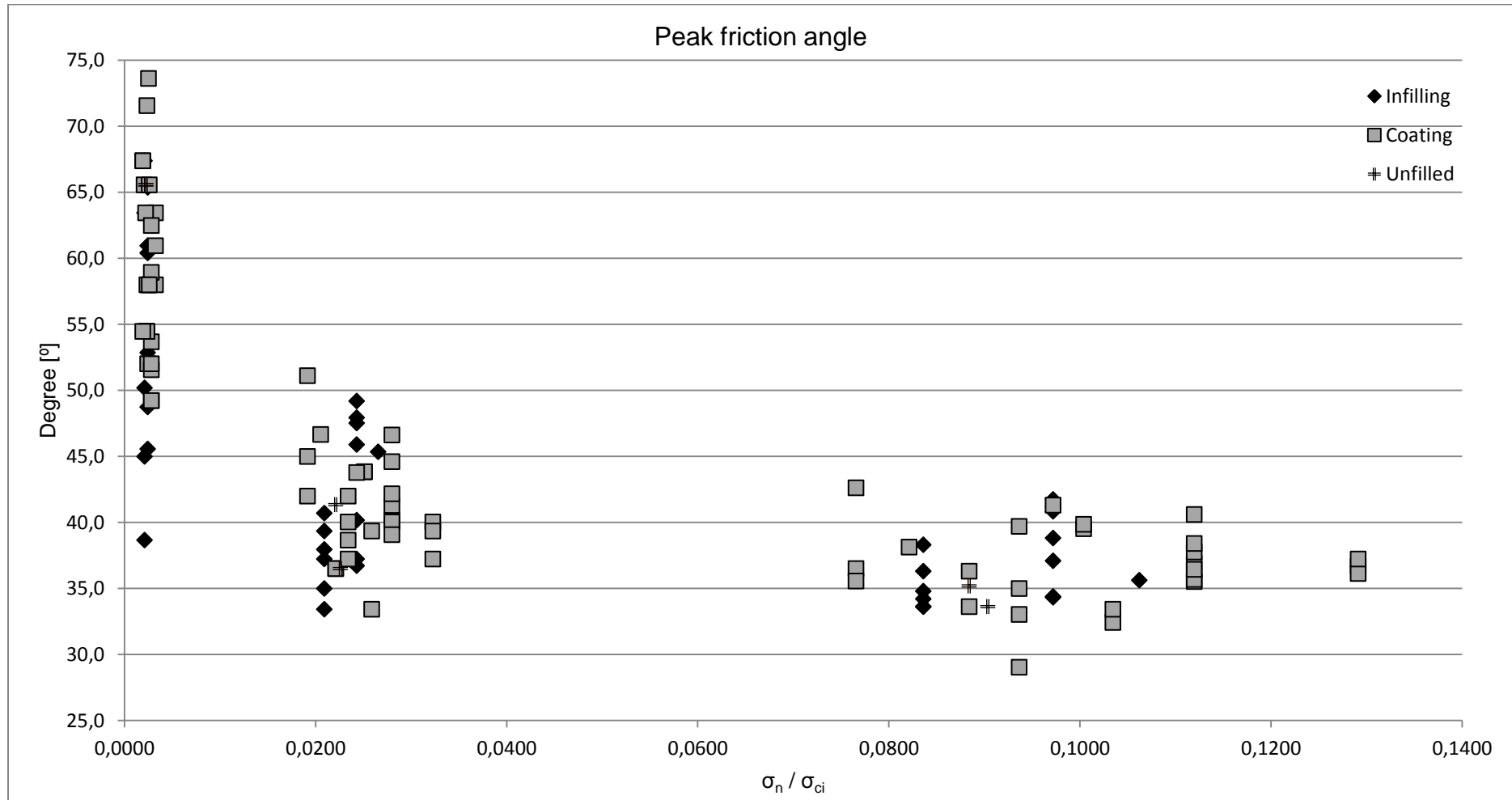


Figure C: The peak friction angle is plotted against the ratio between the normal stress and the uniaxial compressive strength according to the infilling characteristics of the fracture.

Figure D does not show obvious influences of the JRC on the peak friction angle. The JRC values are randomly scattered at all stress levels.

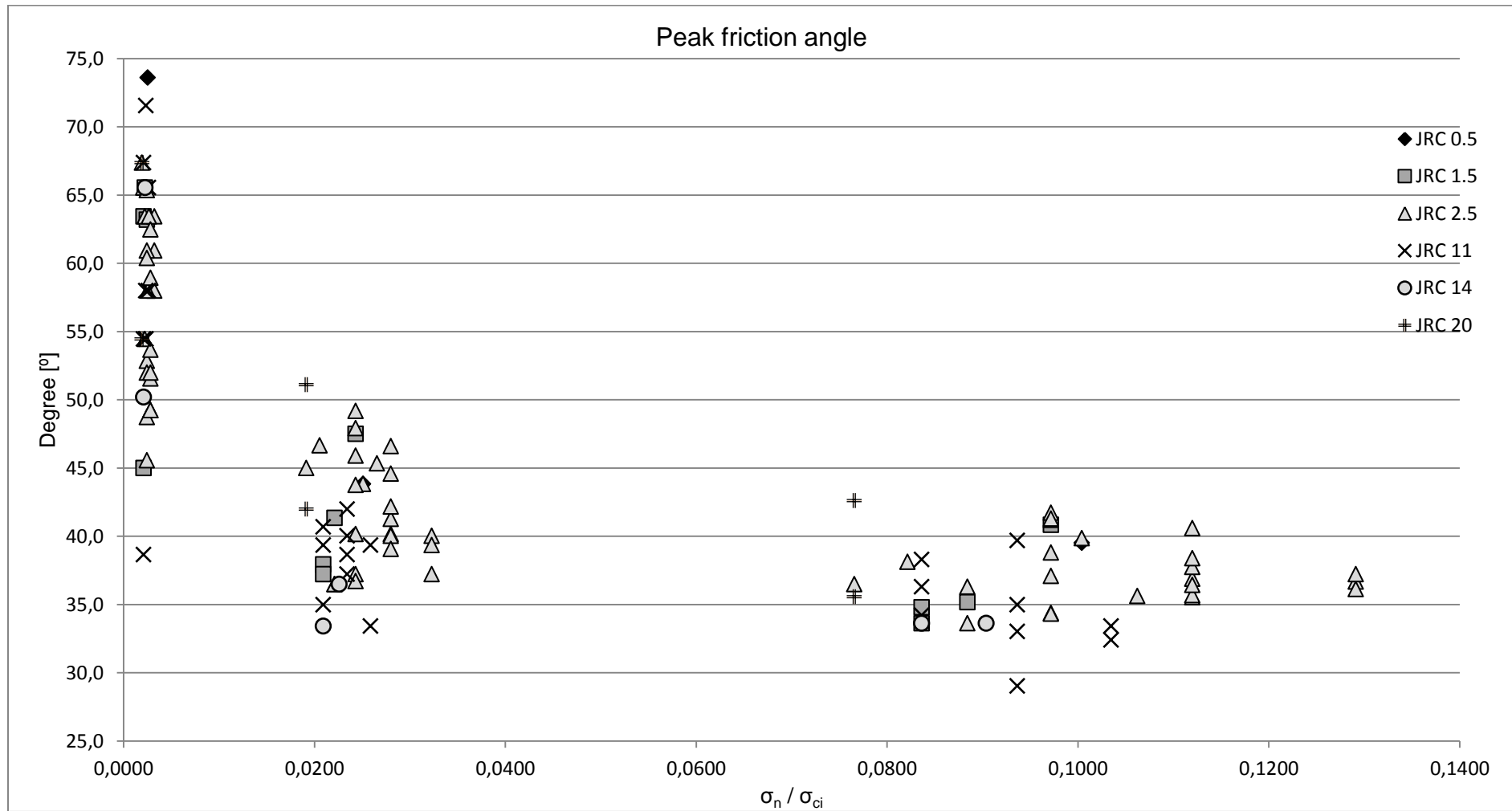


Figure D: The peak friction angle is plotted against the ratio between the normal stress and the uniaxial compressive strength according to the JRC value.

In Figure E, the peak dilation angle decreases with increasing normal load but no patterns or trends can be related to the JRC values.

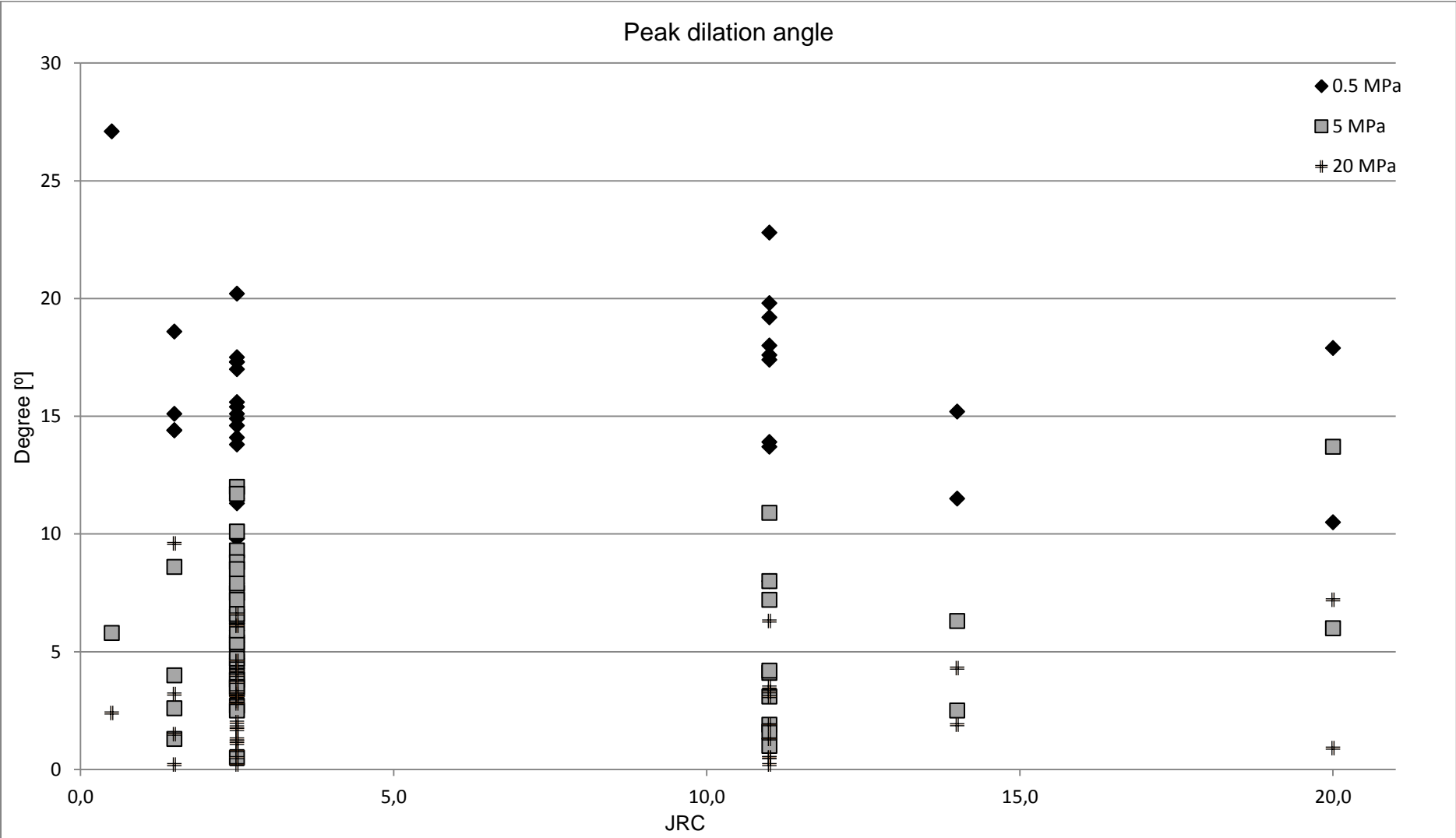


Figure E : The peak dilation angle is plotted to the JRC, distinguished by normal stress level groups.

Figure F does not exhibit a clear trend of the relation between the peak dilation angle and the fracture width.

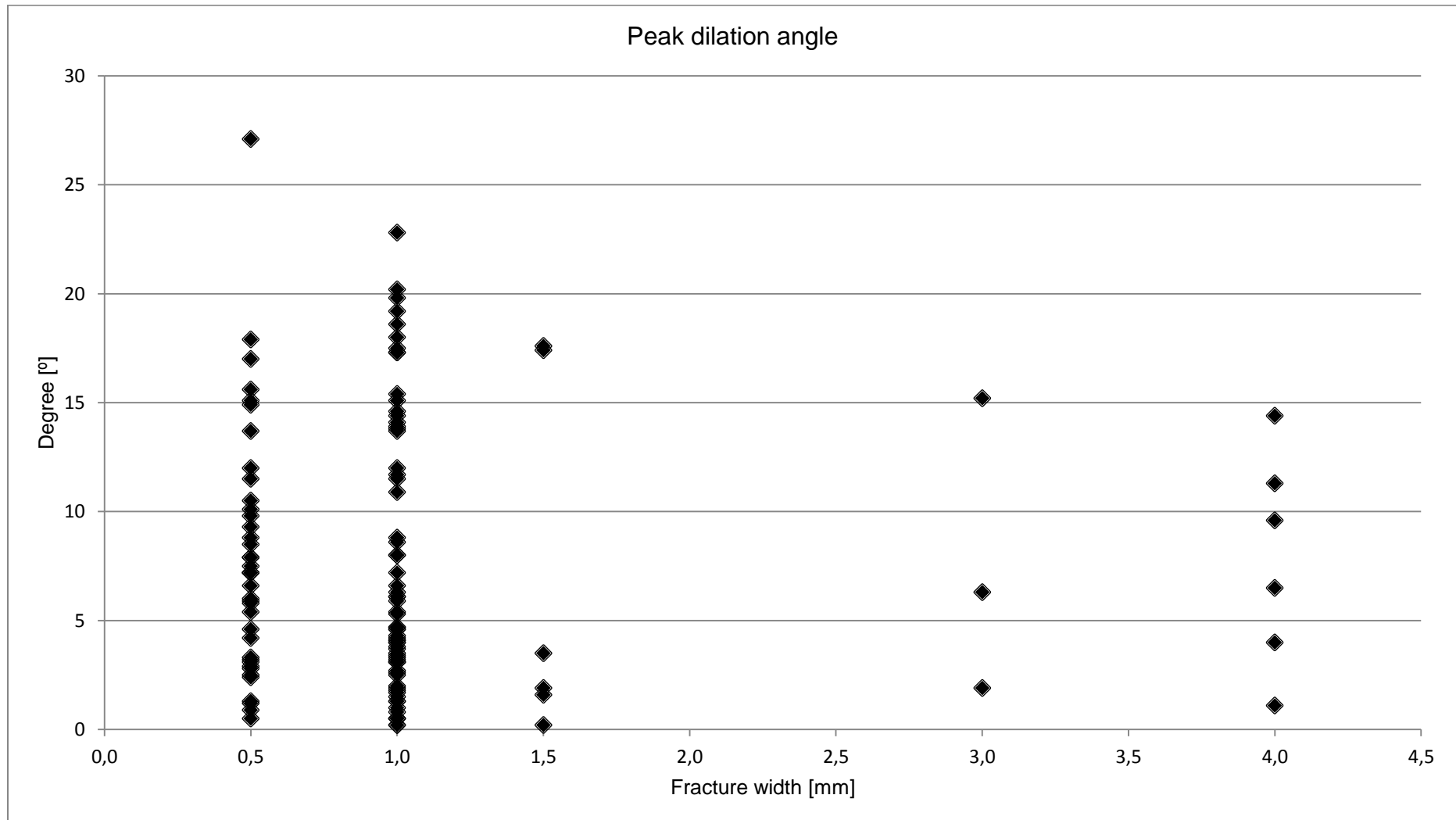


Figure F: The peak dilation angle plotted against the fracture width.

Figure G confirms that the peak dilation angle decreases with increasing normal stress. In low stress condition, a trend of the importance of the infilling characteristics can be distinguished. In high stress, the infilling and coating properties are randomly scattered.

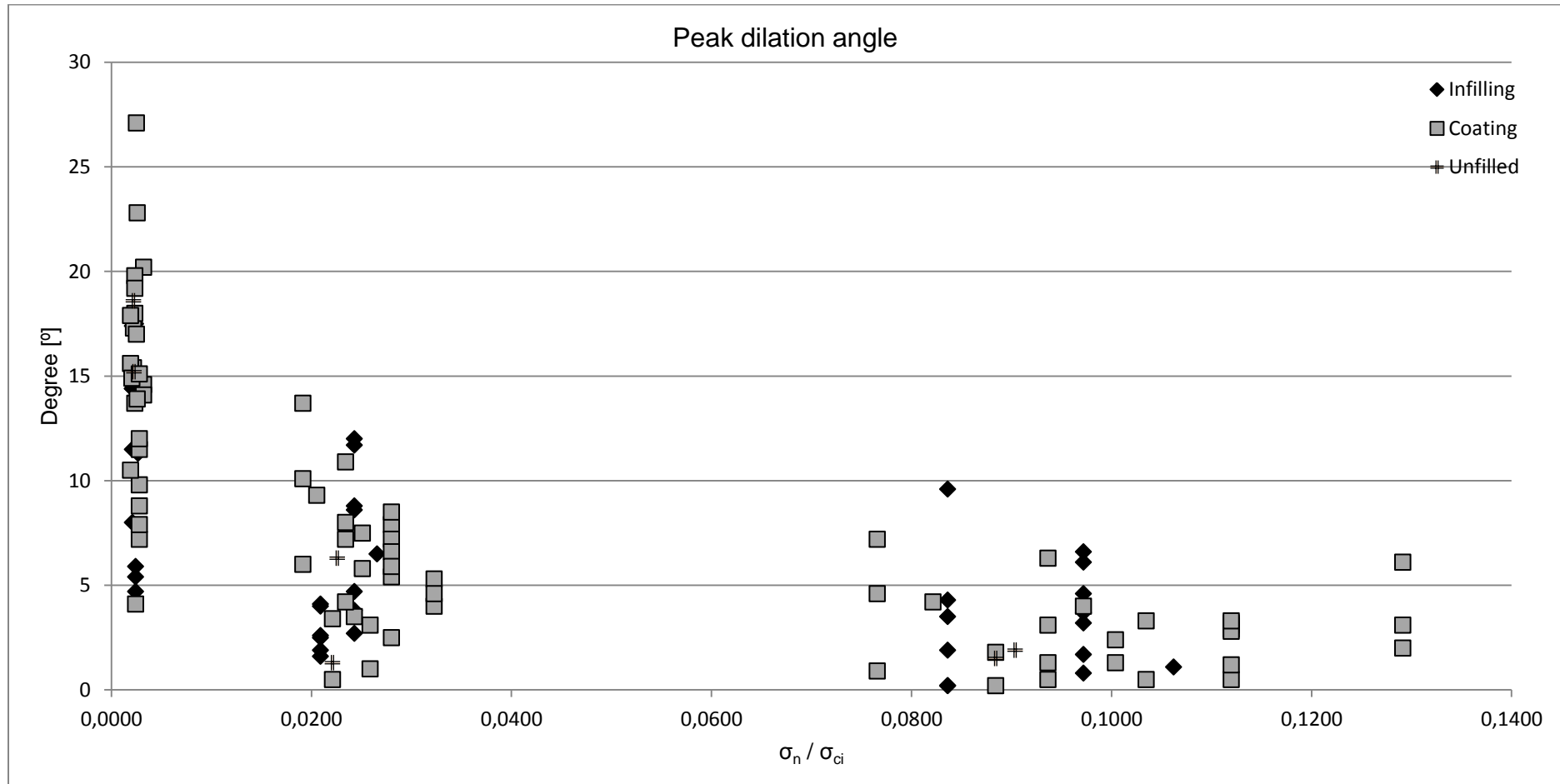


Figure G: The peak dilation angle plotted against the ratio between the normal stress and the uniaxial compressive strength, divided by infilling characteristics.

Figure H does not show obvious interactions between the normal stiffness and JRC value.

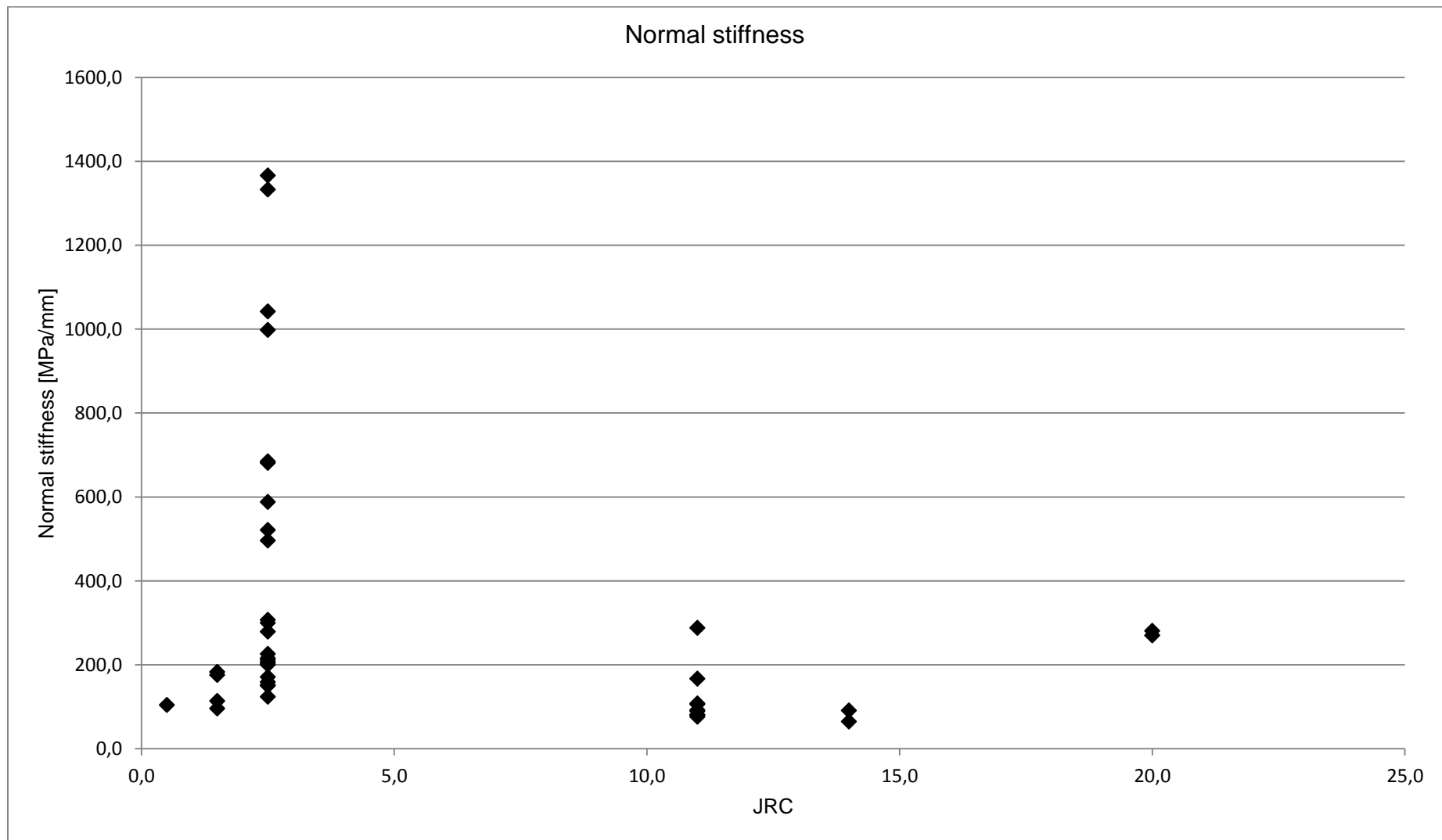


Figure H: The normal stiffness is plotted against the JRC value.

In Figure I, the 0.5 millimetre opening does not contain infilling material and has a widespread scatter of normal stiffness. Wider fractures display lower values of the normal stiffness.

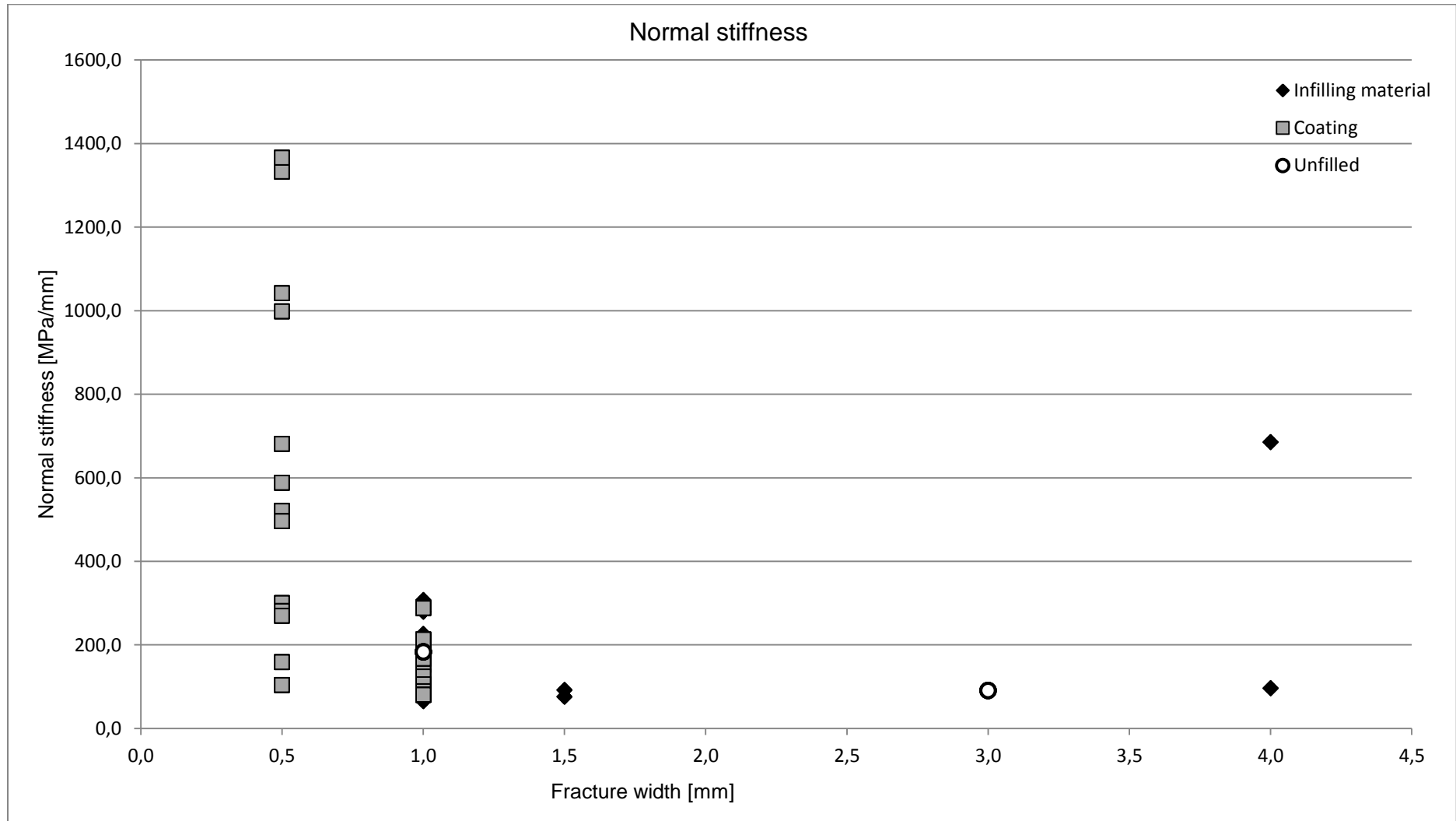


Figure I: The normal stiffness is plotted against the fracture width, divided by the infilling characteristics.

Figure J shows that the shear stiffness increases with higher normal load but no trend concerning the JRC values can be established.

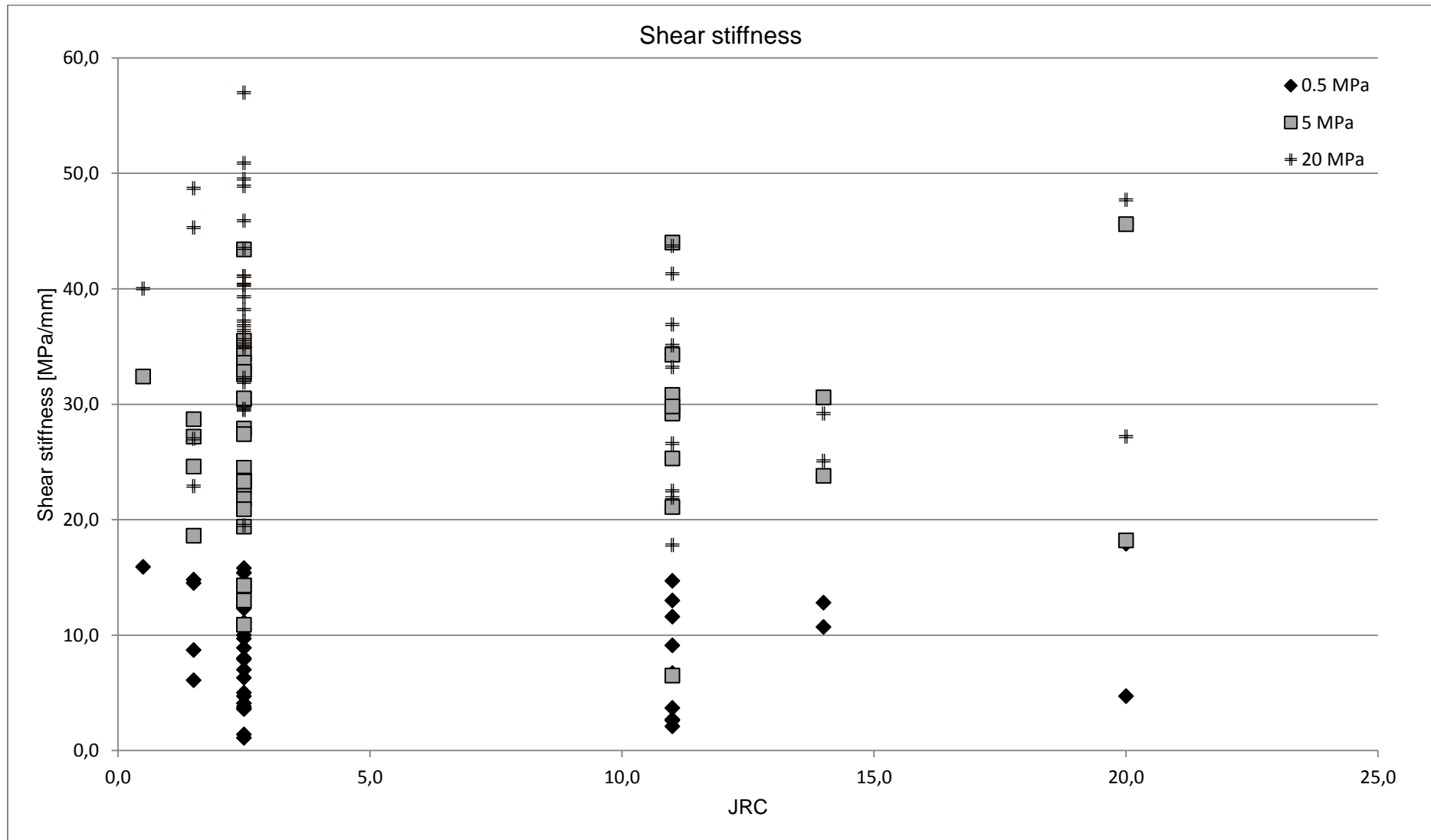


Figure J: The shear stiffness is plotted against the JRC value, divided by groups of normal load used during the direct shear tests.

The Figure K shows that wider fractures contain thicker infilling characteristics, except the 3 millimetre opening. No trends between the shear stiffness and fracture width can however be distinguished.

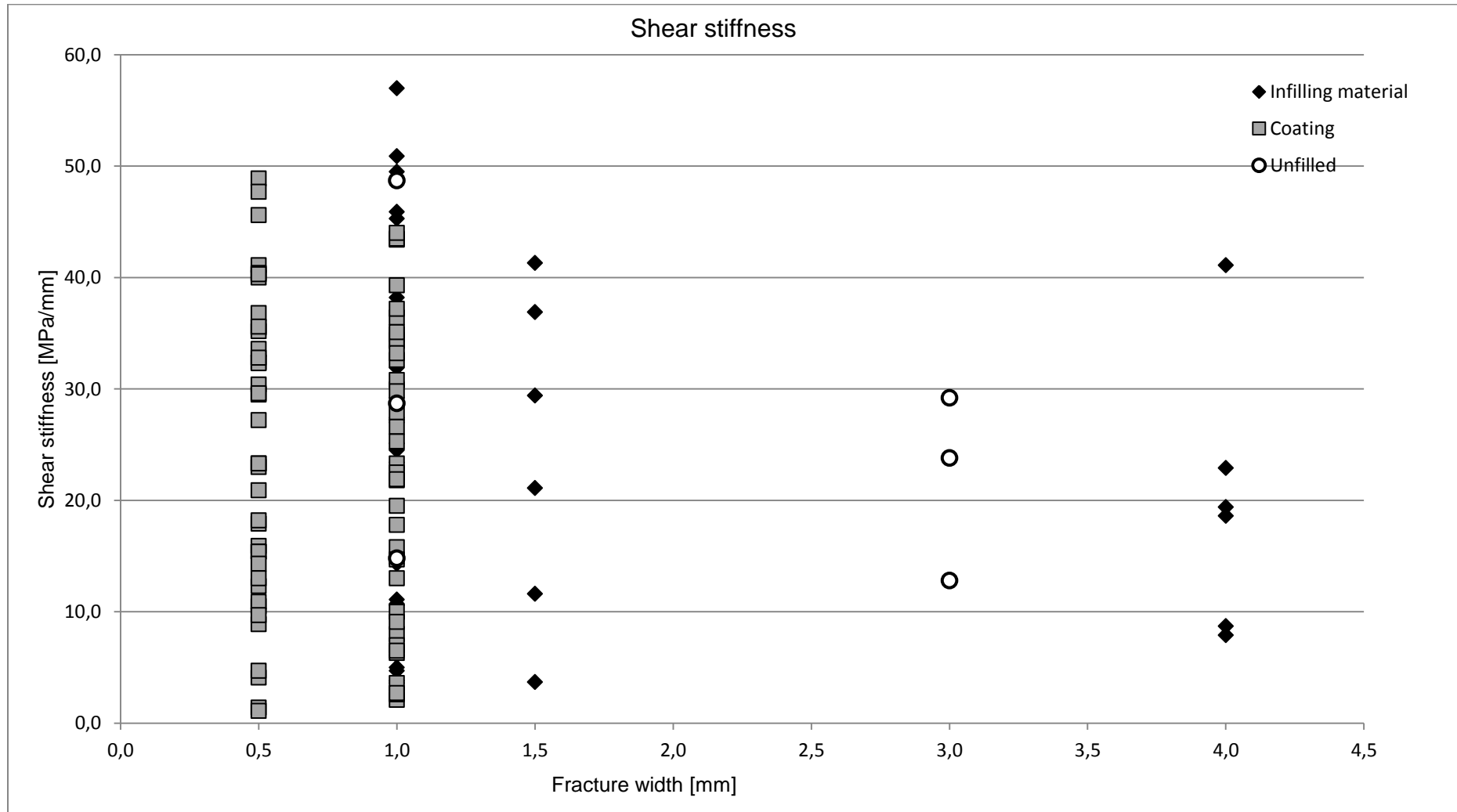


Figure K: The shear stiffness is plotted against the fracture width, divided by infilling characteristics.